JOURNAL OF PETROLOGY | VOLUME 42 | NUMBER 8 | PAGES 1567–1593 | 2001

Sources and Fluids in the Mantle Wedge below Kamchatka, Evidence from Across-arc Geochemical Variation

T. CHURIKOVA[1,2], F. DORENDORF[1] AND G. WÖRNER[1]*

[1]GEOCHEMISCHES INSTITUT, GOLDSCHMIDTSTRASSE 1, 37077 GÖTTINGEN, GERMANY

[2]INSTITUTE OF VOLCANIC GEOLOGY AND GEOCHEMISTRY, PIIP AVENUE 9, PETROPAVLOVSK-KAMCHATSKY, RUSSIA

RECEIVED DECEMBER 15, 1999; REVISED TYPESCRIPT ACCEPTED MARCH 12, 2001

Major and trace element and Sr–Nd–Pb isotopic variations in mafic volcanic rocks hve been studied in a 220 km transect across the Kamchatka arc from the Eastern Volcanic Front, over the Central Kamchatka Depression to the Sredinny Ridge in the back-arc. Thirteen volcanoes and lava fields, from 110 to 400 km above the subducted slab, were sampled. This allows us to characterize spatial variations and the relative amount and composition of the slab fluid involved in magma genesis. Typical Kamchatka arc basalts, normalized for fractionation to 6% MgO, display a strong increase in large ion lithophile, light rare earth and high field strength elements from the arc front to the back-arc. Ba/Zr and Ce/Pb ratios, however, are nearly constant across the arc, which suggests a similar fluid input for Ba and Pb. La/Yb and Nb/Zr increase from the arc front to the back-arc. Rocks from the Central Kamchatka Depression range in $^{87}Sr/^{86}Sr$ from 0·70334 to 0·70366, but have almost constant Nd isotopic compositions ($^{143}Nd/^{144}Nd$ 0·51307–0·51312). This correlates with the highest U/Th ratios in these rocks. Pb-isotopic ratios are mid-ocean ridge basalt (MORB)-like but decrease slightly from the volcanic front to the back-arc. The initial mantle source ranged from N-MORB-like in the volcanic front and Central Kamchatka Depression to more enriched in the back-arc. This enriched component is similar to an ocean-island basalt (OIB) source. Variations in $(CaO)_{6·0}$–$(Na_2O)_{6·0}$ show that degree of melting decreases from the arc front to the Central Kamchatka Depression and remains constant from there to the Sredinny Ridge. Calculated fluid compositions have a similar trace element pattern across the arc, although minor differences are implied. A model is presented that quantifies the various mantle components (variably depleted N-MORB-mantle and enriched OIB-mantle) and the fluid compositions added to this mantle wedge. The amount of fluid added ranges from 0·7 to 2·1%. The degree of melting changes from ~20% at the arc front to <10% below the back-arc region. The rocks from volcanoes of the northern part of the Central Kamchatka Depression—to the north of the transect considered in this study—are significantly different in their trace element compositions compared with the other rocks of the transect and their source appears to have been enriched by a component derived from melting of the edge of the ruptured slab.

KEY WORDS: *geochemical zonation; Kamchatka; subduction zone; mantle sources; fluid*

INTRODUCTION

The major volumetric source of arc magmatism is the mantle wedge above the subducted oceanic plate. Melting in subduction zones is triggered by interaction between this mantle wedge and slab-derived hydrous fluids and/or melts. Slab fluids are known to be enriched in large ion lithophile elements (LILE, e.g. Cs, Rb, K, Ba, Pb) and light rare earth elements (LREE) but depleted in high field strength elements (HFSE, e.g. Nb, Ta, Zr, Hf) and heavy rare earth elements (HREE; e.g. Ayers, 1998; Brenan *et al.*, 1995). In rare cases, silica-rich melts are produced by partial melting of the subducted oceanic plate (Defant & Drummond, 1990). Compared with hydrous fluids, such melts are high in Mg, Si and Sr/Y, enriched in

Extended dataset can be found at http://www.petrology.oupjournals.org

*Corresponding author. Telephone: +49-551-393-971. E-mail: gwoerne@gwdg.de.

all incompatible elements, including the HFSE, strongly depleted in the HREE, and have mid-ocean ridge basalt (MORB)-like isotopic composition.

The incompatible trace element patterns of primitive island-arc volcanic rocks were used by Pearce (1983) and McCulloch & Gamble (1991), among others, to estimate the slab fluid contribution to the mantle source. A problem in this approach is that additional factors such as differences in melting degree and contributions from subducted sediments, the subcontinental lithosphere or the crust may have a large influence on the trace element patterns. These factors may vary from arc to arc and are mainly related to crustal thickness, mantle fertility, and the composition and thermal state of the subducted plate (Plank & Langmuir, 1988, 1993; Pearce & Parkinson, 1993; Arculus, 1994) as well as the amount and compositions of subducted sediments (Plank & Langmuir, 1993). By studying cross-arc variations in major and trace element and isotopic composition of primitive arc rocks, some of these variables can be evaluated. Such studies were performed successfully for Japan (Shibata & Nakamura, 1997) and the Kurile Islands (Avdeiko *et al.*, 1991). Previous studies of across-arc variations on Kamchatka (Volynets, 1994; Tatsumi *et al.*, 1995; Hochstaedter *et al.*, 1996; Kepezhinskas *et al.*, 1997) gave rather ambiguous results, owing largely to a limited database.

The Kamchatka Peninsula forms the northern part of the Kurile–Kamchatka volcanic arc in the NW Pacific Ocean and represents one of the most volcanically active regions on Earth. More than 200 Quaternary volcanoes, including 28 active ones (Melekestsev *et al.*, 1991), have been identified on Kamchatka. Interest in Kamchatka has focused in particular on the large magma production rates, the abundance of Recent to historical eruptions and the mafic compositions of lavas compared with other arcs. The most intense Holocene activity is found in the Kluchevskaya Volcanic Group of the Central Kamchatka Depression (CKD), with Kluchevskoy volcano (4750 m) being the most productive arc volcano in the world (55×10^6 tons magma/a, after Melekestsev *et al.*, 1991). Additionally, it was shown previously (Tsvetkov *et al.*, 1989; Kersting & Arculus, 1995; Turner *et al.*, 1998) that the amount of the sedimentary component is limited, offering the chance to investigate a relatively simple system.

We analysed volcanic rocks from a densely sampled east–west transect across Kamchatka (Fig. 1) for major and trace element, and Sr, Nd and Pb isotope compositions to assess the changes across the arc and to evaluate their possible causes. The transect has the potential to test existing models of slab dehydration (Tatsumi & Eggins, 1995; Schmidt & Poli, 1998), melt generation (Plank & Langmuir, 1988; Pearce & Parkinson, 1993), and changing slab fluids with depth.

GEOLOGICAL SETTING AND SAMPLING

The Kamchatka arc is located at the NE convergent boundary of the Eurasian and Pacific plates, below which the Pacific plate is at present being subducted at the rate of ~9 cm/a (Geist & Scholl, 1994). With it, the Emperor Seamounts chain is also being subducted below Kamchatka. Volcanic activity on Kamchatka dates back to the Cretaceous. The current plate-tectonic configuration, however, formed only in the Late Miocene to Early Pliocene. Plateau basalts, partly with intra-plate characteristics, were erupted from the Pliocene to Lower Pleistocene. A remarkable increase in volcanism occurred in the Upper Pleistocene to Holocene (Luchitsky, 1974). Active volcanism continues southward to the Kurile island arc. The northern termination of volcanic activity at Shiveluch volcano is related to the Aleutian–Kamchatka triple junction (Gorelchik *et al.*, 1997; Volynets *et al.*, 1997*b*; Yogodzinski *et al.*, 2000). Here the plate boundary changes from convergent in the south (Pacific–Eurasia) to strike-slip motion in the north (Pacific–North America). Extinct volcanoes of 2–15 Ma age (Kepezhinskas *et al.*, 1997) occur further north and are related to a short-lived spreading centre in the Komandorsky basin (Baranov *et al.*, 1991).

Quaternary arc volcanism on Kamchatka (Fig. 1) comprises from east to west three zones parallel to the trench: (1) the Eastern Volcanic Front (EVF); (2) the Central Kamchatka Depression (CKD) with the Kluchevskaya Group and three more northern volcanoes of the Northern Central Kamchatka Depression (NCKD); (3) the Western Volcanic Zone of the Sredinny Ridge (SR). The SR represents the now extinct Miocene volcanic front, which switched to a back-arc position after the accretion of the Kronotsky terrane and the formation of the Recent active volcanic front.

Geophysical data for the Kamchatka crust are limited. Seismic observations (Balesta, 1991) show crustal thickness in Kamchatka to vary from south to north from 20 km to 42 km. Across the arc at the latitude of the CKD, crustal thickness varies from 30 km below the Sredinny Ridge to 40–42 km below Kluchevskoy volcano. This is somewhat unexpected, because the CKD is considered to be a rift-like structure and should be related to crustal thinning. The characteristic feature of this thickened crustal section below the Kluchevskaya Group area is a 10–12 km thick crust–mantle transition zone (Balesta, 1991). Most probably, the geophysically determined Moho does not represent the compositional transition

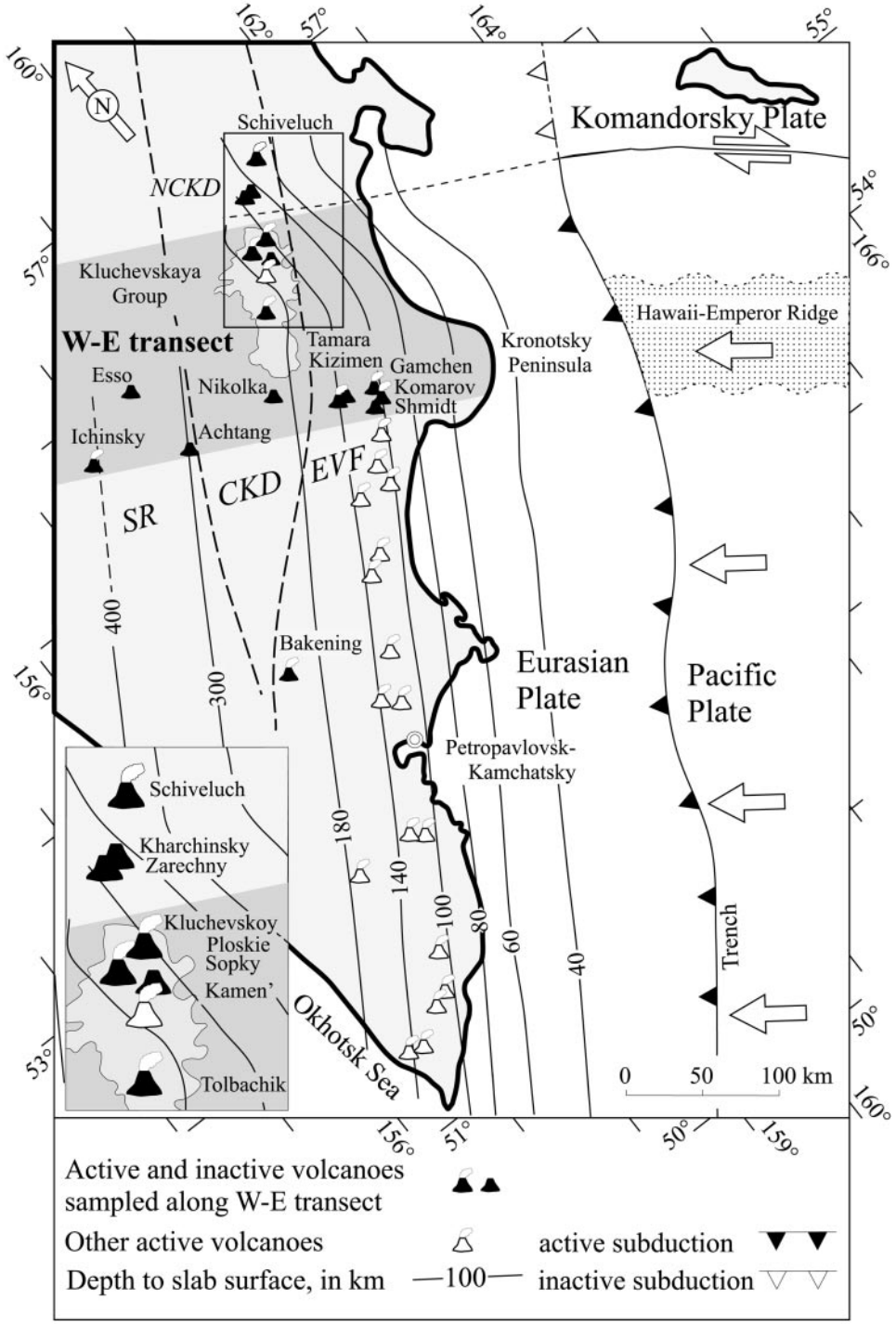

Fig. 1. General plate tectonic position of the Kamchatka arc and the location of the transect in northern Kamchatka (shaded band). The depth to the Benioff zone is from Gorbatov (1997). Sampled volcanoes are marked by shaded symbols. CKD borders are from Masurenkov (1991). SR, Sredinny Ridge; CKD, Central Kamchatka Depression; EVF, Eastern Volcanic Front. Inset shows detail of the NCKD (North Central Kamchatka Depression).

from crust to mantle because of massive basaltic underplating below the rifted CKD crust. Evidence for magma chambers within the crust–mantle transition has been obtained from seismic studies of the lower crust and upper mantle below several Kamchatka volcanoes; depths of crustal chambers range from

1·5–2·0 km below the Avachinsky and Tolbachinsky volcanoes to 10–20 km for Bezymianny volcano (Balesta, 1991).

The depth of the seismic zone of the descending slab increases from 100–140 km below the Eastern Volcanic Front to 400 km below Ichinsky volcano (Fedotov, 1991; Gorbatov, 1997). The dip angle of the slab changes from 55° in the south to only 35° to the north of the Kronotsky Peninsula, resulting in a shift of the volcanic front to the west. This change in the dip angle is connected with the subduction of the Hawaii–Emperor ridge (Gorbatov, 1997).

We have sampled a 220 km traverse of 13 Upper Pleistocene and Holocene stratovolcanoes and two large lava fields with several monogenetic cones. The transect starts from the frontal zone (Komarov, Gamchen, Shmidt, Kizimen, Tamara cone) through the Kluchevskaya Group (Kluchevskoy, Tolbachik, Ploskie Sopky, Kamen, Shiveluch, Kharchinsky, Zarechny, Nikolka) into the back-arc with monogenetic volcanic centres at Achtang and Esso, and the isolated Ichinsky stratovolcano. The across-arc distance, over which Holocene volcanic activity and large stratovolcanoes occur, is comparably wide and possibly the largest in the world today. Other wide arcs (such as Peru or Alaska) do not have such productive and recent back-arc activity. We note that this large across-arc range of Quaternary volcanism in Kamchatka is found only in the region where the Emperor Seamounts chain is being subducted.

The rocks studied are mostly Upper Pleistocene to Holocene in age. Rare exceptions belong to the Pliocene to Lower Pleistocene plateau basalts and one Middle Pleistocene shield volcano. A detailed description of the sampling areas, samples and petrography, and the complete analytical data may be downloaded from the *Journal of Petrology* Web site at http://www.petrology.oupjournals.org, and are also available from the Göttingen Web site (http://www.uni-geochem.gwdg.de) The depth of the seismofocal zone and location of the volcanoes are shown in Fig. 1.

ANALYTICAL TECHNIQUES

Major elements and some trace elements (Sc, V, Cr, Co, Ni, Zn, Ga, Sr, Zr, Ba) were determined on 178 samples by X-ray fluorescence (XRF) analysis of glass discs, prepared with a lithium tetraborate flux. Fe_2O_3 was determined titrimetrically with $KMnO_5$ and the loss on ignition (LOI) by weight difference at heating to 1100°C. Analytical errors for major elements are around 1% (except for Fe and Na, 2%; and LOI, ~10%) and for trace elements around 5%.

Additional trace elements were analysed by inductively coupled plasma mass spectrometry (ICPMS) on 90 samples. Whole-rock powders (~100 mg) were dissolved in Teflon beakers with a mixture of HF and $HClO_4$ under pressure, and after evaporation were redissolved in HNO_3 for the measurement. Rock standards JB3 and JA2 were analysed continuously together with samples to check the external reproducibility. From this we estimate the error for Nb and Ta to be about 15–20%, and for other trace elements <10%.

Isotope ratios for Sr, Nd and Pb were measured with a Finnigan MAT 262 RPQ II+ mass spectrometer at Göttingen. The same ICPMS dissolution procedure was used. Whole-rock powders (~100 mg) were dissolved for Sr and Nd, and ~200–300 mg of crushed rock chips, leached with 2·6N HCl, were used for Pb isotope determination.

The Sr- and Nd-isotope ratios were corrected for mass fractionation to $^{86}Sr/^{88}Sr = 0{\cdot}1194$ and $^{146}Nd/^{144}Nd = 0{\cdot}7219$ and normalized to values for NBS987 (0·710245), and La Jolla (0·511847), respectively. Measured values of these standards over the period of the study were $0{\cdot}710262 \pm 24$ and $0{\cdot}511847 \pm 20$. From measurement of standards for Sr and Nd (12 and 17) and repeated measurements of samples (13 for Sr and four for Nd), external errors (2σ) are estimated at <0·004% for Sr and Nd isotopes. Lead isotopes were corrected to NBS981 standard (Todt *et al.*, 1984). Normalization of our data to recommended values was performed using a mass fractionation factor of 0·122%. From measurement of 13 standards and repeated measurements of samples, total errors (2σ) <0·1% for Pb isotopes were determined. Procedural blanks for Sr, Nd and Pb (<1 ng, <0·03 ng and <0·5 ng, respectively) were insignificant.

RESULTS AND DISCUSSION

Major and trace elements

Major and trace element compositions for representative samples from the northern Kamchatka transect are listed in Table 1. Rocks of the EVF, including Kizimen volcano, belong to the low- to medium-K series (Fig. 2). The rocks of the back-arc (SR) are medium to high-K. Near Ichinsky volcano we found HFSE-enriched basalts with within-plate affinities (here: basalts of within-plate type—WPT) at the base of the stratovolcano, which itself is composed of andesitic to rhyodacitic rocks of typical island-arc basalt (IAB) signature. The largest variations in alkalis are observed for the CKD rocks. They are mostly medium-K, but some samples of Ploskie Sopky and Nikolka volcanoes, as well as some Al-basalts from Tolbachik, are high-K. Northern CKD (NCKD) volcanoes Shiveluch, Kharchinsky and Zarechny erupted high-Mg andesites, containing a slab melt component (Kepezhinskas *et al.*, 1997; Volynets *et al.*, 1997*b*; Yogodzinski *et al.*, 2000).

Table 1: Major and trace element abundances in representative samples from the transect

	Gamchen						Shmidt			Komarov					Kizimen			
	GAM-07 EVF Q3	GAM-12 EVF Q4	GAM-14 EVF Q4	GAM-22 EVF Pliocene	GAM-26 EVF Q2	GAM-28 EVF Q2	SHM-01 EVF Q3-4	SHM-03 EVF Q3-4	SHM-04 EVF Q3-4	KOM-01 EVF Q3	KOM-02 EVF Q3	KOM-06 EVF Q3	KOM-11 EVF Q4	KOM-14 EVF Q3	TAM-01 EVF Q4	KIZ-01 EVF Q4	KIZ-01/1 EVF Q4	KIZ-05 EVF Q4
SiO_2	51·60	54·70	55·80	52·80	50·60	49·80	50·60	59·10	50·90	52·60	53·70	51·70	61·00	53·50	51·40	63·60	49·70	56·20
TiO_2	0·85	0·80	0·86	0·80	1·00	0·83	0·89	0·70	0·77	0·84	0·75	0·83	0·82	0·81	0·83	0·58	1·22	0·89
Al_2O_3	18·61	19·76	18·51	17·20	18·51	17·89	16·17	18·44	18·13	17·15	16·00	16·32	16·48	17·84	15·76	16·17	18·84	17·26
Fe_2O_3	3·43	2·30	3·38	2·49	2·87	2·59	3·75	3·78	2·92	2·20	1·86	2·03	2·19	3·19	9·37	2·41	5·32	3·43
FeO	5·73	4·67	5·39	6·88	8·48	7·96	5·94	3·49	6·44	7·01	6·48	7·47	4·43	6·24	0·43	3·03	5·56	4·75
MnO	0·18	0·14	0·18	0·19	0·20	0·20	0·18	0·21	0·18	0·18	0·17	0·18	0·14	0·18	0·19	0·13	0·19	0·17
MgO	5·35	2·98	3·62	5·95	4·94	6·24	8·07	2·21	6·91	6·39	7·33	8·20	2·82	5·36	8·43	2·44	5·20	3·99
CaO	9·12	8·44	7·96	9·54	9·93	10·93	10·39	6·99	10·39	9·66	9·36	9·68	6·24	9·33	9·23	5·34	9·25	7·17
Na_2O	2·72	3·18	3·26	2·78	2·60	2·37	2·34	3·60	2·50	2·58	2·55	2·41	3·42	2·83	2·72	3·69	2·74	3·27
K_2O	0·49	0·68	0·33	0·54	0·61	0·66	0·57	0·46	0·57	0·79	0·8	0·68	1·40	0·56	0·73	1·66	0·76	1·14
P_2O_5	0·12	0·12	0·13	0·12	0·11	0·13	0·12	0·06	0·11	0·13	0·12	0·11	0·14	0·12	0·23	0·16	0·17	0·16
LOI	1·58	0·46	0·46	0·60	0·46	0·21	0·45	0·96	0·55	0·41	0·70	0·56	0·32	0·36	0·66	0·61	0·73	1·17
Total	99·78	98·23	99·87	99·88	100·32	99·80	99·47	100·00	100·37	99·94	99·83	100·17	99·40	100·31	99·98	99·82	99·67	99·60
Li	2·2		1·5	2·4	2·5	1·5	9·6	7·7	6·1	7·1	6·8	5·2		7·9	7·9	16·3	14·2	10·2
Be	0·23		0·23	0·25	0·25	0·28	0·41	0·39	0·37	0·34	0·34	0·32		0·29	0·51	0·79	0·52	0·63
Sc	28	21	25	34	35	41	36	18	34	33	35	37	20	30	31	15	26	21
V	230	173	248	269	359	313	257	34	285	274	246	267	171	269	221	114	300	208
Cr	38	10	4	87	26	79	335	0	117	137	309	368	16	11	481	17	15	10
Co	32	17	22	35	38	40	43	7	37	36	33	41	21	36	36	14	30	29
Ni	20	0	4	46	13	30	103	0	54	35	89	119	0	24	166	0	2	7
Zn	72	68	67	84	101	80	78	50	81	79	75	81	72	84	79	55	79	68
Ga	17	20	16	17	21	17	15	16	18	15	15	16	17	17	15	16	17	17
Rb	9	14*	4	8	9	11	15	7	12	18	15	13	36*	9	15	38	14	26
Sr	278	293	263	257	268	331	215	408	287	231	219	240	235	247	380	319	370	330
Y	18	25*	20	19	19	17	21	17	19	24	27	18	33*	21	16	16	21	20
Zr	61	80	62	73	61	54	74	62	60	84	86	74	147	71	86	121	86	102
Nb	1·0	0·0*	0·6	1·1	0·9	0·9	1·6	1·2	1·4	1·5	2·0	1·1	5·0*	1·7	2·4	4·2	2·9	3·5
Cs	0·28		0·10	0·38	0·53	0·41	0·67	0·37	0·56	0·78	0·97	0·59		0·55	0·50	1·5	0·52	0·47
Ba	154	214	117	199	205	327	189	168	241	261	234	226	366	174	358	676	310	458
La	3·91		2·82	4·20	3·61	4·38	3·68	3·99	5·52	4·36	3·83	3·94		4·54	7·62	10·16	5·85	7·73
Ce	11·49		9·41	12·70	10·90	13·07	9·72	11·38	13·50	11·75	9·79	9·91		10·41	19·02	22·39	15·18	19·37
Pr	1·67		1·51	1·78	1·54	1·95	1·57	1·79	1·92	1·87	1·69	1·63		1·40	2·69	3·32	2·34	2·76
Nd	8·20		8·01	8·49	7·80	9·47	8·65	8·85	9·75	10·37	10·86	8·72		8·98	13·10	13·54	11·99	12·79
Sm	2·50		2·58	2·56	2·44	2·72	2·51	2·80	3·10	2·89	2·53	2·47		2·78	3·72	2·89	3·36	3·23
Eu	0·84		0·89	0·85	0·83	0·88	0·78	1·01	0·99	0·84	0·72	0·74		0·83	1·11	0·95	1·14	1·04
Gd	2·64		2·84	2·69	2·67	2·69	2·67	2·55	2·90	3·14	3·01	2·61		2·88	3·29	2·58	3·28	2·97
Tb	0·46		0·50	0·47	0·47	0·44	0·47	0·50	0·59	0·47	0·42	0·41		0·49	0·52	0·36	0·54	0·44
Dy	2·95		3·23	3·06	3·05	2·79	2·85	3·20	3·35	3·23	2·79	2·78		2·98	3·38	2·28	3·33	2·94
Ho	0·66		0·73	0·69	0·67	0·61	0·67	0·63	0·62	0·69	0·63	0·61		0·63	0·67	0·5	0·74	0·65
Er	1·97		2·18	2·08	2·04	1·79	2·18	1·86	1·93	2·13	2·00	1·79		2·12	2·06	1·46	2·18	1·85
Tm	0·28		0·32	0·31	0·30	0·26	0·31	0·30	0·36	0·33	0·31	0·28		0·32	0·32	0·20	0·30	0·26
Yb	1·89		2·15	2·08	1·95	1·68	1·90	2·18	2·35	2·00	1·80	1·70		2·02	2·05	1·39	2·00	1·72
Lu	0·29		0·34	0·32	0·30	0·26	0·27	0·31	0·28	0·32	0·30	0·28		0·30	0·31	0·24	0·29	0·28
Hf	1·60		1·65	1·99	1·53	1·45	1·91	1·52	1·73	2·19	2·11	1·75		1·93	2·27	1·91	1·99	1·88
Ta	0·08		0·06	0·07	0·08	0·08	0·10	0·09	0·09	0·09	0·07	0·06		0·08	0·19	0·21	0·17	0·17
Tl	0·04		0·01	0·05	0·05	0·04	0·02	0·03	0·04	0·08	0·11	0·06		0·08	0·03	0·27	0·10	0·10
Pb	2·18		0·98	1·78	1·83	1·68	1·63	2·36	2·33	2·42	2·08	1·91		1·75	2·15	5·30	1·95	3·01
Th	0·57		0·21	0·60	0·48	0·58	0·57	0·28	0·61	0·82	0·84	0·82		0·52	0·91	3·19	1·02	1·42
U	0·26		0·14	0·28	0·23	0·32	0·29	0·18	0·44	0·36	0·42	0·33		0·27	0·45	1·45	0·49	0·79

Table 1: continued

	Kizimen			Ploskie Sopky			Ploskie Sopky High-K				Tolbachik		Tolbachik High-K			Kamen		Kluchevskoy	
	KIZ-19 EVF Q3	KIZ-24 EVF Q4	KIZ-24/1 EVF Q4	2330 CKD Q3	1-90 CKD Q3	3-90 CKD Q4	5-90 CKD Q4	306-84 CKD Q4	PLO-16 CKD Q3	128 CKD Q4	TOL-6/6 CKD Q4	655 CKD 1975	TOL-6/3 CKD Q4	201 CKD 1941	22-8 CKD 1975	2310 CKD Q4	2311 CKD Q1	KLU-02 CKD Q4	KLU-03 CKD Q4
SiO_2	50·30	54·70	51·60	50·41	49·95	50·10	56·72	51·60	58·20	50·86	51·40	50·46	50·90	50·21	51·10	50·54	51·83	54·20	53·70
TiO_2	1·20	1·03	1·28	0·99	0·97	0·86	1·41	1·66	1·19	1·24	1·15	0·95	1·22	1·18	1·59	1·12	0·96	1·11	0·85
Al_2O	$16·50_3$	17·44	17·91	15·27	17·09	15·79	16·27	16·93	18·54	15·00	14·51	13·42	14·57	14·17	17·51	16·83	17·16	18·13	15·33
Fe_2O	$2·97_3$	3·07	4·29	3·47	3·32	3·00	2·39	2·18	1·78	2·20	3·64	2·14	3·59	3·60	2·25	3·05	3·36	2·58	2·06
FeO	8·01	5·49	5·78	6·64	6·70	6·68	6·20	7·82	4·58	7·39	6·09	7·16	6·31	6·46	7·20	6·81	5·69	5·98	6·42
MnO	0·21	0·17	0·19	0·19	0·17	0·17	0·18	0·16	0·11	0·17	0·18	0·17	0·18	0·17	0·16	0·18	0·16	0·16	0·16
MgO	5·22	4·16	4·42	7·97	6·88	7·84	2·95	4·70	1·76	8·05	8·86	9·67	9·10	9·61	4·34	7·13	6·39	5·21	8·88
CaO	9·59	8·18	9·13	10·30	10·52	10·26	6·15	8·00	6·82	9·94	10·29	11·60	10·19	9·83	8·30	10·32	9·43	8·24	9·40
Na_2O	2·70	3·18	3·03	2·59	2·66	2·57	4·34	3·41	3·84	2·80	2·54	2·37	2·73	2·61	3·46	2·74	3·12	3·62	2·89
K_2O	0·71	1·10	0·87	0·87	0·87	0·99	2·23	2·05	2·54	1·36	1·15	0·85	1·29	1·26	1·97	0·57	0·68	1·18	0·76
P_2O_5	0·21	0·17	0·19	0·22	0·18	0·22	0·49	0·59	0·67	0·36	0·32	0·21	0·35	0·34	0·56	0·15	0·16	0·22	0·16
LOI	1·87	0·47	0·85	0·67	0·41	0·65	0·49	0·69	0·49	0·57	0·60	0·63	0·36	0·47	0·79	0·58	0·70	0·32	0·33
Total	99·48	99·16	99·53	99·58	99·72	99·13	99·82	99·80	100·52	99·93	100·73	99·63	100·78	99·91	99·22	100·03	99·64	100·96	100·94
Li	3·8	8·5	11·7	7·4	7·0	7·1	18·4	14·6		9·6		7·2		10·2	14·7	7·9	8·4	13·2	8·3
Be	0·44	0·56	0·56	0·57	0·52	0·45	1·31	1·45		0·88		0·59		0·90	1·41	0·40	0·42	0·63	0·50
Sc	35	22	33	39	38	32	26	24	17	35	41	38	36	33	22	38	32	30	36
V	316	246	324	308	346	294	246	288	176	275	283	270	276	271	270	318	262	260	240
Cr	42	24	21	462	279	312	90	81	2	408	430	418	438	569	165	231	225	45	426
Co	37	27	27	45	39	39	22	32	10	41	41	40	41	47	30	32	33	37	37
Ni	25	2	0	84	46	82	2	45	1	105	158	99	177	168	45	33	44	39	151
Zn	94	72	80	97	71	87	104	110	81	91	85	75	89	87	99	82	81	88	79
Ga	18	19	17	15	16	16	19	19	19	16	16	16	16	16	19	17	16	18	16
Rb	9	21	16	15	15	18	43	55	75*	34	29*	18	31*	34	52	8	11	18	12
Sr	276	328	335	363	478	450	374	352	354	319	309	292	308	305	362	300	336	393	324
Y	32	20	23	20	17	16	33	33	53*	26	27*	19	28*	27	32	22	20	21	15
Zr	104	99	90	76	66	65	199	210	339	133	119	79	130	124	199	70	77	104	81
Nb	4·1	3·1	3·2	1·6	1·3	1·0	4·1	5·7	11·0*	3·4	3·0*	1·5	5·0*	3·1	4·8	1·4	1·5	1·8	1·2
Cs	0·31	0·79	0·59	0·37	0·32	0·38	1·31	1·74		0·97		0·46		0·91	1·58	0·22	0·35	0·47	0·42
Ba	164	419	323	307	332	279	692	485	808	324	303	229	322	296	467	168	240	398	290
La	6·49	6·52	7·02	6·73	6·60	6·49	16·50	18·00		11·37		6·47		10·50	17·00	4·32	5·39	7·55	5·41
Ce	19·11	16·57	18·10	16·61	17·61	15·00	40·60	44·21		29·32		16·33		27·03	41·87	11·95	14·02	19·26	13·63
Pr	2·73	2·83	2·59	2·72	2·75	2·29	6·32	6·69		4·54		2·72		4·37	6·42	2·03	2·31	3·16	2·17
Nd	13·11	12·73	13·08	13·28	12·66	12·21	28·38	30·32		21·03		13·59		20·14	29·03	10·72	11·38	14·88	10·37
Sm	3·86	3·25	3·91	3·75	3·55	3·25	7·09	7·26		5·37		3·85		5·29	7·14	3·34	3·32	4·07	2·94
Eu	1·14	1·08	1·27	1·15	1·08	0·97	1·90	1·91		1·51		1·12		1·46	1·84	1·10	1·05	1·26	0·90
Gd	4·04	3·12	3·53	3·56	3·22	3·11	6·30	6·37		4·82		3·56		4·58	6·22	3·49	3·25	3·75	2·89
Tb	0·70	0·47	0·63	0·60	0·51	0·44	1·00	1·01		0·77		0·58		0·75	0·97	0·64	0·56	0·62	0·45
Dy	4·37	3·08	3·88	3·58	2·96	2·70	5·79	5·80		4·58		3·50		4·25	5·66	3·90	3·47	3·82	3·66
Ho	0·945	0·76	0·75	0·73	0·61	0·61	1·16	1·17		0·94		0·73		0·84	1·17	0·83	0·71	0·77	0·61
Er	2·89	1·97	2·23	2·09	1·77	1·64	3·38	3·37		2·61		2·00		2·52	3·47	2·39	2·04	2·22	1·68
Tm	0·42	0·27	0·34	0·32	0·25	0·22	0·49	0·51		0·39		0·29		0·37	0·49	0·35	0·31	0·34	0·26
Yb	2·77	1·72	2·38	2′·02	1·55	1·57	3·20	3·24		2·54		1·89		2·27	3·19	2·26	2·05	2·13	1·61
Lu	0·42	0·30	0·32	0·31	0·24	0·25	0·48	0·49		0·38		0·28		0·34	0·48	0·34	0·31	0·34	0·25
Hf	2·80	2·10	2·17	2·08	1·82	1·59	4·78	4·93		3·34		2·05		3·02	4·75	1·89	1·97	2·49	1·88
Ta	0·21	0·14	0·19	0·12	0·32	0·07	0·21	0·29		0·39		0·08		0·14	0·28	0·17	0·14	0·09	0·09
Tl	0·05	0·09	0·10	0·04	0·05	0·06	0·11	0·08		0·08		0·06		0·05	0·06	0·05	0·02	0·06	0·05
Pb	2·03	2·73	2·63	3·11	3·13	3·20	7·80	10·14		3·87		2·03		3·23	7·49	2·19	2·44	3·26	3·06
Th	0·59	1·57	0·91	0·52	0·98	0·75	1·85	2·15		1·64		0·49		0·95	2·31	0·30	0·50	0·77	0·61
U	0·38	0·77	0·61	0·37	0·39	0·33	1·17	1·27		0·76		0·32		0·65	1·26	0·26	0·33	0·49	0·41

	Kluchevskoy													Nikolka			Kharchinsky	
	KLU-04 CKD Q4	KLU-05 CKD Q4	KLU-06 CKD Q4	KLU-07 CKD Q4	KLU-08 CKD Q4	KLU-09 CKD Q4	KLU-10 CKD Q4	KLU-11 CKD Q4	KLU-12 CKD Q4	KLU-13 CKD Pliocene	KLU-14 CKD Pliocene	KLU-15 CKD Miocene	KLU-16 CKD Q3	8868 CKD Q3	8878 CKD Q4	8883 CKD Q4	8837 NCKD Q4	8840 NCKD Q3
SiO_2	52·20	52·50	53·50	53·50	52·90	52·70	52·60	52·60	54·00	54·20	54·30	53·40	53·70	55·24	55·97	51·07	50·08	50·64
TiO_2	1·07	0·99	0·89	0·84	1·00	0·96	0·97	0·97	1·11	1·13	1·10	0·86	0·94	1·25	0·85	1·39	0·88	0·90
Al_2O_3	15·99	16·35	15·25	14·59	16·66	15·55	15·72	15·82	18·08	18·52	17·85	14·60	15·86	17·76	16·69	18·37	13·46	13·86
Fe_2O_3	2·81	2·29	2·53	2·59	2·84	3·01	2·31	2·31	2·89	3·23	3·48	3·71	2·66	4·42	1·78	4·79	3·95	4·49
FeO	6·34	6·51	6·25	5·88	6·00	6·01	6·63	6·79	5·61	5·33	5·20	4·94	6·13	4·12	5·70	4·96	5·42	4·74
MnO	0·17	0·16	0·16	0·16	0·16	0·17	0·17	0·17	0·16	0·16	0·17	0·17	0·17	0·14	0·14	0·17	0·16	0·16
MgO	7·70	7·49	8·33	9·44	7·43	8·31	8·20	8·23	5·03	4·61	4·94	8·67	7·32	2·46	4·19	3·56	12·29	11·30
CaO	9·39	9·37	9·70	9·59	9·41	9·71	9·72	9·79	8·14	8·01	8·18	10·03	9·38	7·18	7·40	8·20	9·62	9·62
Na_2O	3·13	3·18	2·84	2·78	3·15	2·98	2·87	2·97	3·60	3·60	3·47	2·74	2·95	3·48	3·30	3·56	2·69	2·84
K_2O	0·71	0·79	0·76	0·74	0·80	0·66	0·65	0·63	1·19	1·20	1·17	0·91	0·94	2·16	1·16	1·36	0·89	0·95
P_2O_5	0·19	0·19	0·16	0·15	0·20	0·17	0·17	0·16	0·22	0·23	0·22	0·17	0·18	0·33	0·17	0·61	0·18	0·19
LOI	0·51	0·48	0·31	0·43	0·51	0·54	0·45	0·40	0·40	0·43	0·22	0·38	0·30	2·23	1·05	0·82	0·69	0·74
Total	100·22	100·31	100·68	100·69	101·06	100·77	100·46	100·84	100·43	100·66	100·31	100·58	100·54	100·76	98·42	99·84	100·31	100·42
Li	7·8	9·1	8·1	8·6	8·9	8·3	7·5	7·9	13·9	13·3	13·5	9·8	10·9	19·2	5·0	15·5	7·4	7·6
Be	0·58	0·62	0·48	0·47	0·62	0·50	0·49	0·54	0·66	0·68	0·71	0·51	0·55	1·00	0·57	1·05	0·49	0·48
Sc	35	35	34	36	31	35	35	37	21	27	27	38	33	22	29	25	30	31
V	248	234	245	244	247	250	255	262	259	267	258	246	255	282	227	265	252	257
Cr	283	240	341	500	221	343	318	321	31	6	33	431	256	202	330	148	862	789
Co	39	39	40	40	35	38	39	36	33	30	33	40	32	21	24	28	50	53
Ni	99	106	107	166	88	104	108	109	31	14	21	110	93	10	1	22	255	262
Zn	84	80	81	78	80	78	81	81	87	88	89	77	85	86	81	99	81	77
Ga	15	18	16	16	17	17	19	18	18	19	18	15	19	18	18	18	17	17
Rb	10	12	11	12	12	10	9	9	19	19	19	16	15	46	19	41	12	11
Sr	293	315	299	312	319	290	290	287	397	403	374	333	341	419	416	469	476	487
Y	19	18	16	15	19	18	18	19	22	22	23	18	19	27	18	30	16	16
Zr	100	99	81	77	98	87	85	85	104	105	107	75	87	142	93	176	66	69
Nb	1·7	1·7	1·2	1·3	1·8	1·4	1·5	1·4	2·0	1·9	2·0	1·3	1·5	3·0	1·7	4·4	1·2	1·1
Cs	0·36	0·46	0·28	0·39	0·39	0·33	0·31	0·32	0·51	0·48	0·58	0·44	0·43	2·00	0·24	0·23	0·28	0·18
Ba	223	259	283	280	261	243	224	228	434	428	402	307	344	743	478	689	331	331
La	6·12	6·69	5·03	5·31	6·72	5·54	5·32	5·36	8·43	8·20	8·42	6·80	6·09	14·38	8·12	20·60	6·49	6·62
Ce	16·27	17·09	13·01	13·14	17·47	14·29	14·22	14·58	21·11	21·31	21·48	16·97	15·09	35·71	19·4	51·29	17·01	17·06
Pr	2·62	2·77	2·14	2·13	2·83	2·38	2·34	2·46	3·39	3·54	3·61	2·71	2·49	5·28	2·98	7·66	2·69	2·79
Nd	12·45	12·65	10·24	10·27	12·90	11·19	11·40	11·57	15·75	15·64	16·75	12·25	11·87	24·72	14·19	33·92	13·55	13·72
Sm	3·54	3·41	2·91	2·99	3·50	3·07	3·21	3·25	4·14	4·14	4·27	3·36	3·35	6·33	3·67	7·65	3·68	3·68
Eu	1·07	1·04	0·94	0·93	1·07	1·02	1·02	0·97	1·27	1·29	1·33	1·02	1·06	1·65	1·12	1·93	1·09	1·09
Gd	3·52	3·35	3·01	2·87	3·35	3·18	3·20	3·20	3·77	3·76	3·88	3·04	3·32	5·41	3·26	6·16	3·17	3·20
Tb	0·57	0·54	0·48	0·46	0·56	0·53	0·55	0·56	0·63	0·65	0·64	0·51	0·54	0·88	0·54	0·94	0·52	0·53
Dy	3·27	3·07	2·91	3·46	3·36	3·42	3·42	3·84	3·82	4·04	3·05	3·42	4·90	3·14	5·33	2·87	2·92	2·87
Ho	0·79	0·69	0·64	0·59	0·72	0·68	0·70	0·70	0·82	0·81	0·83	0·66	0·71	0·98	0·64	1·07	0·58	0·60
Er	2·27	1·98	1·82	1·73	2·06	1·95	2·06	2·04	2·36	2·34	2·38	1·84	1·99	2·85	1·83	3·05	1·67	1·71
Tm	0·33	0·30	0·27	0·25	0·30	0·28	0·31	0·31	0·34	0·36	0·34	0·28	0·29	0·41	0·28	0·44	0·24	0·24
Yb	2·10	1·91	1·67	1·61	1·98	1·84	1·98	1·96	2·15	2·16	2·26	1·69	1·94	2·64	1·71	2·86	1·45	1·45
Lu	0·32	0·29	0·25	0·24	0·30	0·29	0·30	0·30	0·34	0·32	0·33	0·26	0·29	0·39	0·25	0·43	0·21	0·23
Hf	2·35	2·25	1·98	1·86	2·32	2·08	2·07	2·03	2·55	2·56	2·57	1·89	2·04	4·02	2·51	4·38	2·05	2·09
Ta	0·12	0·11	0·07	0·08	0·11	0·09	0·10	0·10	0·14	0·16	0·14	0·09	0·09	0·49	0·34	0·50	0·13	0·10
Tl	0·03	0·05	0·03	0·05	0·04	0·03	0·03	0·04	0·07	0·06	0·05	0·03	0·13	0·18	0·08	0·05	0·03	0·02
Pb	2·70	3·07	2·74	2·79	2·82	2·73	2·39	2·26	3·39	3·36	3·53	2·79	3·04	6·50	3·72	7·19	3·07	2·84
Th	0·49	0·56	0·55	0·59	0·60	0·48	0·48	0·44	0·80	0·78	0·79	0·71	0·65	1·70	0·65	2·47	0·45	0·44
U	0·33	0·40	0·40	0·40	0·38	0·34	0·32	0·31	0·49	0·46	0·49	0·39	0·42	1·23	0·51	1·38	0·31	0·32

Table 1: continued

	Shiveluch			Zarechny	Achtang			Cinder cones around Esso				Ichinsky						
	2569 NCKD Q4	2577 NCKD Q4	2585 NCKD Q4	90093 NCKD Q4	ACH-01 SR Q4	ACH-02 SR Q4	ACH-03 SR Q4	ESO-01 SR Q4	ESO-04 SR Q1?	ESO-08 SR Q4	ESO-11 SR Q4	6250 SR Q4	ICH-19 SR Q4	ICH-02 SR Q4	6334/1 SR Q3	ICH-25 SR Q4	ICH-28 SR Q3	ICH-29 SR Q3
SiO_2	54·99	52·65	55·93	51·71	54·40	51·20	53·40	53·70	52·95	50·60	52·50	51·99	50·40	54·90	59·10	65·50	55·80	53·00
TiO_2	0·71	0·83	0·69	0·85	0·90	0·94	0·98	0·84	0·87	0·98	0·82	0·85	0·89	1·19	0·80	0·54	0·90	1·11
Al_2O_3	14·97	15·19	15·16	13·64	17·28	15·97	17·02	18·22	18·01	17·78	17·49	14·70	20·21	16·74	16·98	15·81	16·85	17·55
Fe_2O_3	5·17	6·00	2·62	1·78	2·28	2·94	2·31	3·06	2·27	2·39	2·73	3·01	3·11	2·02	1·66	1·49	1·89	2·82
FeO	2·80	3·30	4·88	7·34	5·19	5·84	5·77	5·03	5·73	6·43	5·82	5·62	5·08	5·87	4·76	2·47	5·18	5·21
MnO	0·15	0·17	0·15	0·17	0·15	0·16	0·15	0·16	0·15	0·16	0·15	0·16	0·14	0·15	0·12	0·09	0·13	0·14
MgO	7·01	6·78	7·42	10·43	5·13	7·89	6·15	5·16	5·48	6·51	6·36	8·41	4·88	4·80	3·29	1·73	4·97	5·04
CaO	8·54	9·30	8·56	9·35	7·62	9·61	8·19	8·36	8·55	9·75	9·16	10·07	9·77	7·44	6·37	4·16	7·71	8·46
Na_2O	3·24	3·26	3·39	2·70	3·28	2·86	3·19	3·28	3·17	2·92	2·91	2·66	3·17	3·73	3·86	4·04	3·57	3·49
K_2O	1·33	1·29	1·29	1·05	1·54	1·16	1·34	1·14	1·15	0·88	1·04	1·46	1·05	1·49	1·89	2·54	1·31	1·27
P_2O_5	0·23	0·32	0·23	0·19	0·31	0·29	0·28	0·23	0·22	0·23	0·22	0·23	0·25	0·48	0·34	0·17	0·32	0·37
LOI	0·59	0·61	0·29	0·613	1·10	0·66	0·76	0·31	0·67	0·59	0·29	0·63	0·40	0·60	1·11	0·55	0·51	0·59
Total	99·73	99·71	100·60	99·81	99·21	99·53	99·54	99·49	99·21	99·21	99·49	99·79	99·34	99·41	100·27	99·08	99·15	99·05
Li	8·7	9·2	8·4	7·2	7·2	5·4	9·2	9·2	8·1	3·1	5·0	6·6	7·1	11·5	12·3	29·0	10·4	10·1
Be	0·74	0·81	0·69	0·49	0·77	0·56	0·69	0·70	0·70	0·47	0·55	0·81	0·70	1·05	1·15	1·11	0·93	0·79
Sc	27	32	29	32	23	30	22	22	27	30	29	32	25	23	13	14	22	24
V	185	262	206	255	196	243	216	217	231	261	242	243	219	194	164	100	172	216
Cr	555	188	366	840	99	337	163	107	121	186	205	346	33	74	51	12	97	72
Co	30	34	27	46	26	37	31	32	34	34	38	39	30	26	19	10	31	33
Ni	57	28	75	141	49	112	90	58	60	69	77	92	45	30	25		77	64
Zn	72	95	69	75	74	78	76	75	76	81	77	73	74	92	82	52	74	87
Ga	16	17	17	15	19	17	19	16	18	17	15	16	20	18	18	17	18	17
Rb	24	23	21	18	25	21	21	21	20	14	19	25	18	20	33	49	20	20
Sr	512	525	508	378	598	530	583	657	641	592	620	503	722	596	526	366	532	581
Y	15	18	16	17	22	21	21	18	18	19	16	18	15	22	20	13	18	17
Zr	81	80	81	71	122	93	115	80	79	70	74	95	93	177	173	174	157	138
Nb	2·1	1·5	2·0	1·3	6·4	3·9	5·5	2·9	3·1	1·7	2·0	3·7	3·6	8·2	7·0	6·2	6·0	6·8
Cs	0·74	0·70	0·43	0·34	0·44	0·41	0·36	0·48	0·46	0·36	0·36	0·38	0·21	0·30	0·58	1·21	0·40	0·39
Ba	347	324	341	290	576	373	461	502	493	369	443	443	454	583	659	696	469	440
La	8·27	7·01	7·71	5·71	12·79	8·76	10·60	8·18	7·89	6·11	7·34	9·03	8·22	19·14	18·93	16·14	16·53	13·54
Ce	18·70	16·91	18·11	14·45	33·09	24·03	28·53	22·01	21·26	17·72	20·06	22·24	19·00	46·27	44·31	34·01	36·40	34·35
Pr	2·94	2·75	2·77	2·38	4·21	3·27	3·72	2·88	2·80	2·54	2·66	3·30	2·86	6·43	5·80	4·55	4·69	4·87
Nd	13·68	13·12	12·84	11·65	17·79	14·66	16·12	12·81	12·41	12·08	11·78	15·19	14·02	28·21	23·38	17·10	20·71	20·81
Sm	3·47	3·65	3·25	3·27	4·02	3·62	3·77	3·09	3·04	3·15	2·92	3·82	3·55	6·27	4·96	3·58	5·13	4·91
Eu	1·02	1·11	0·96	0·99	1·20	1·11	1·14	0·97	0·95	1·02	0·93	1·11	1·19	1·79	1·31	0·98	1·43	1·48
Gd	3·00	3·28	2·88	3·07	3·47	3·30	3·34	2·63	2·60	2·85	2·54	3·31	3·12	5·36	4·06	3·01	4·38	4·16
Tb	0·49	0·53	0·46	0·52	0·51	0·50	0·47	0·40	0·39	0·45	0·39	0·52	0·49	0·79	0·61	0·45	0·73	0·61
Dy	2·87	3·11	2·73	3·09	3·02	3·04	2·87	2·31	2·32	2·64	2·24	3·10	2·79	4·69	3·50	2·80	4·15	3·72
Ho	0·57	0·67	0·56	0·63	0·63	0·64	0·61	0·48	0·48	0·54	0·45	0·61	0·55	0·92	0·70	0·58	0·78	0·74
Er	1·63	1·86	1·56	1·84	1·82	1·89	1·79	1·43	1·44	1·58	1·34	1·73	1·61	2·62	2·02	1·59	2·23	1·95
Tm	0·26	0·28	0·24	0·27	0·27	0·27	0·24	0·20	0·21	0·23	0·19	0·26	0·24	0·37	0·30	0·24	0·36	0·27
Yb	1·64	1·86	1·63	1·76	1·70	1·71	1·52	1·35	1·34	1·47	1·23	1·67	1·48	2·48	1·93	1·73	2·31	1·83
Lu	0·25	0·28	0·24	0·27	0·27	0·27	0·26	0·21	0·20	0·22	0·18	0·25	0·23	0·37	0·30	0·28	0·31	0·29
Hf	2·26	2·08	2·19	1·91	2·99	2·37	2·74	2·09	2·04	2·82	1·89	2·50	2·28	4·26	4·17	3·42	3·86	3·28
Ta	0·12	0·15	0·14	0·08	0·30	0·18	0·23	0·15	0·15	0·10	0·10	0·42	0·24	0·46	0·60	0·45	0·39	0·32
Tl	0·08	0·06	0·14	0·08	0·13	0·10	0·11	0·09	0·10	0·08	0·07	0·13	0·04	0·09	0·17	0·26	0·11	0·08
Pb	5·17	3·89	3·77	2·87	5·11	3·25	4·03	4·59	4·30	2·66	3·99	4·25	3·43	5·57	7·47	8·09	5·91	4·10
Th	1·02	0·80	1·25	0·59	1·22	0·71	1·03	0·69	0·69	0·38	0·70	1·45	0·76	1·53	2·45	4·05	1·82	1·32
U	0·52	0·49	0·54	0·41	0·63	0·38	0·47	0·41	0·40	0·26	0·43	0·71	0·39	0·59	0·99	1·75	0·84	0·50

	Ichinsky										Ichinsky, WPT								
	ICH-30 SR Q1	ICH-31 SR Q4	ICH-32 SR Q4	ICH-33 SR Q4	ICH-40 SR Q3	ICH-46 SR Q3	ICH-49 SR Q3	ICH-54 SR Q4	ICH-64 SR Q4	ICH-72 SR Q4	6283 SR Q3-4	ICH-03 SR Q1	ICH-05 SR Q1	ICH-07 SR Q3?	ICH-08 SR Q3?	ICH-10 SR Q3?	ICH-11 SR Q3?	ICH-13 SR Q3?	ICH-69 SR Q4
SiO_2	58·30	54·50	53·80	61·80	68·30	62·10	59·10	55·60	67·40	57·10	49·53	53·10	47·40	49·00	48·70	47·80	49·80	52·70	50·50
TiO_2	0·77	0·91	1·24	0·71	0·56	0·71	0·70	0·96	0·53	1·11	1·64	1·43	1·85	1·79	1·69	1·80	2·06	1·52	1·48
Al_2O_3	17·03	17·61	16·78	16·10	15·58	16·79	16·52	18·11	15·68	17·38	16·66	17·29	16·81	16·59	16·48	16·42	17·44	17·32	16·83
Fe_2O_3	1·81	2·49	2·12	1·58	1·06	2·30	2·23	2·22	1·35	2·41	9·52	2·17	3·87	3·51	7·33	3·77	8·84	2·46	5·41
FeO	4·39	4·91	5·88	3·66	1·49	2·92	3·51	4·77	2·23	4·80	0·89	5·98	6·44	6·43	2·62	6·52	1·92	5·80	4·17
MnO	0·12	0·13	0·15	0·12	0·09	0·10	0·11	0·13	0·09	0·13	0·16	0·15	0·17	0·17	0·16	0·17	0·18	0·15	0·17
MgO	3·39	4·60	5·20	3·00	0·74	2·08	3·27	4·22	1·54	3·93	6·76	4·90	7·38	7·19	7·35	8·64	4·54	4·52	6·94
CaO	6·71	8·08	7·48	5·35	2·12	4·97	6·28	7·92	3·56	7·01	8·75	7·35	9·83	8·57	9·30	8·51	7·38	7·37	8·92
Na_2O	3·70	3·47	3·91	3·89	4·69	4·00	3·35	3·73	4·37	3·79	3·76	3·93	3·57	3·80	3·40	3·43	4·12	4·02	3·69
K_2O	1·53	1·31	1·49	2·19	3·80	2·48	2·11	1·74	3·03	1·79	138	2·03	1·22	1·46	1·44	1·38	1·99	2·23	1·33
P_2O_5	0·29	0·30	0·48	0·25	0·13	0·21	0·21	0·38	0·17	0·37	0·49	0·49	0·47	0·59	0·48	0·51	0·67	0·50	0·59
LOI	0·94	0·69	0·92	0·583	0·33	1·80	1·44	1·00	0·60	0·90	0·60	0·47	0·35	0·30	0·40	0·38	0·46	0·29	0·37
Total	98·98	99·01	99·44	99·23	98·89	100·49	98·83	100·78	100·56	100·71	100·14	99·28	99·37	99·40	99·35	99·33	99·39	98·87	100·39
Li	15·2	12·3	9·3	23·3	23·6	10·9	11·9	12·2		16·8	9·8	12·8	5·6	7·3	5·1	6·2	8·0	17·5	8·1
Be	0·82	0·86	1·14	1·11	1·58	1·00	0·95	1·02		0·99	1·71	1·30	0·98	1·02	1·06	1·16	1·58	1·51	1·09
Sc	21	24	22	15	8	16	20	22	11	23	27	21	27	24	27	24	20	20	28
V	168	199	188	125	31	141	153	179	85	184	241	200	262	241	239	235	215	195	245
Cr	38	66	108	56	4	3	44	48	16	49	247	61	129	174	206	187	5	47	163
Co	16	26	31	18	1	14	19	26	10	19	38	26	45	40	41	46	29	26	40
Ni	29	62	74	31	0	6	32	41	2	38	94	39	68	110	98	184	11	36	113
Zn	71	79	92	65	55	61	62	80	50	75	95	80	85	86	87	85	84	80	93
Ga	17	18	19	18	16	18	17	20	17	18	18	18	19	18	20	18	19	20	20
Rb	23	22	23	41	83	51	43	32	58*	25	19	31	17	21	24	19	26	37	19
Sr	518	559	588	427	298	435	475	645	345	544	672	606	690	688	634	686	738	616	709
Y	15	16	21	16	17	15	16	18	18*	19	24	20	19	20	20	20	25	22	23
Zr	148	128	169	170	259	150	143	163	189	176	152	198	145	164	154	147	215	208	164
Nb	4·8	5·6	10·6	6·8	12·2	5·1	5·2	7·0	10·0*	9·6	13·2	18·7	17·2	16·4	17·2*	15·3	27·2	21·9	13·7
Cs	0·42	0·49	0·44	0·98	1·54	1·20	1·05	0·75		0·35	0·24	0·61	0·20	0·32	0·43	0·29	0·40	0·71	0·34
Ba	556	449	472	646	969	701	677	575	809	559	469	542	317	419	431	403	494	549	501
La	16·19	13·24	20·29	16·61	22·15	13·33	15·49	16·92		16·42	17·04	23·53	18·93	20·76	18·71	17·01	27·43	20·69	20·25
Ce	36·96	28·72	46·57	34·35	47·61	29·14	30·55	36·98		38·02	42·86	53·59	43·35	49·94	42·21	38·40	57·82	44·99	46·72
Pr	5·02	4·03	6·18	4·61	6·21	3·95	3·97	4·93		5·56	5·94	6·95	5·82	6·67	5·72	5·34	7·48	6·39	6·45
Nd	19·96	19·06	27·25	19·38	24·19	16·71	17·97	23·19		23·22	26·19	28·30	25·59	28·57	24·75	25·30	33·37	27·77	29·38
Sm	4·90	4·55	6·39	4·11	5·24	3·84	4·32	5·15		4·92	6·07	6·45	6·42	6·70	5·65	5·58	7·56	5·58	6·64
Eu	1·41	1·29	1·81	1·12	1·34	1·06	1·14	1·42		1·47	1·74	1·91	1·99	2·08	1·73	1·79	2·26	1·68	1·91
Gd	3·94	4·12	5·12	3·66	4·11	3·42	3·73	4·41		4·46	5·10	5·38	5·31	5·57	4·67	5·02	6·53	5·23	5·47
Tb	0·65	0·62	0·83	0·55	0·60	0·50	0·60	0·69		0·65	0·78	0·81	0·82	0·81	0·71	0·73	0·99	0·70	0·81
Dy	3·83	3·42	4·59	3·17	3·85	3·09	3·24	3·69		3·88	4·40	4·86	4·68	4·94	3·95	4·07	5·53	4·15	4·61
Ho	0·71	0·67	0·85	0·69	0·77	0·62	0·64	0·72		0·86	0·85	0·91	0·83	0·92	0·75	0·79	1·07	0·90	0·88
Er	2·00	2·01	2·39	1·91	2·15	1·88	2·00	2·12		2·26	2·36	2·42	2·18	2·33	1·99	2·20	2·92	2·53	2·46
Tm	0·31	0·30	0·37	0·29	0·31	0·26	0·30	0·32		0·30	0·34	0·36	0·31	0·32	0·28	0·30	0·44	0·33	0·36
Yb	2·15	1·82	2·43	1·85	2·24	1·81	1·94	2·02		2·01	2·13	2·42	1·99	2·18	1·82	1·83	2·73	2·08	2·32
Lu	0·33	0·27	0·35	0·29	0·37	0·2	0·27	0·29		0·33	0·32	0·37	0·29	0·33	0·28	0·27	0·41	0·33	0·35
Hf	3·87	3·43	4·18	3·54	5·16	3·99	4·05	4·00		4·03	3·54	4·07	3·49	3·70	1·76	3·44	5·03	4·79	3·85
Ta	0·29	0·27	0·51	0·40	0·84	0·40	0·30	0·36		0·46	0·92	1·16	0·84	0·85	0·01	0·55	1·31	1·00	0·69
Tl	0·15	0·12	0·12	0·22	0·23	0·24	0·25	0·13		0·12	0·02	0·12	0·05	0·04	0·73	0·03	0·01	0·04	0·02
Pb	6·55	4·79	5·23	7·17	11·94	7·41	7·40	6·40		5·54	4·62	5·31	2·17	3·13	2·93	2·18	2·89	2·54	4·04
Th	2·10	1·81	1·81	3·34	5·72	3·83	2·74	2·58		2·22	1·40	2·68	1·65	1·68	2·11	1·63	2·89	3·24	1·53
U	0·92	0·77	0·79	1·57	2·31	1·92	1·53	1·16		0·77	0·50	0·91	0·58	0·63	0·68	0·57	0·97	1·10	0·58

EVF, Eastern Volcanic Front; CKD, Central Kamchatka Depression; NCKD, Northern Central Kamchatka Depression; SR, Sredinny Range. Age groups: Q1, 780–1670 ka; Q2, 130–780 ka; Q3, 130–10 ka; Q4, 10 ka to present time; years of activity are given for historical eruptions. All major elements, Sc, V, Cr, Co, Ni, Zn, Ga, Sr, Zr, Ba and elements marked by asterisks were determined by XRF, and other values were determined by ICP-MS.

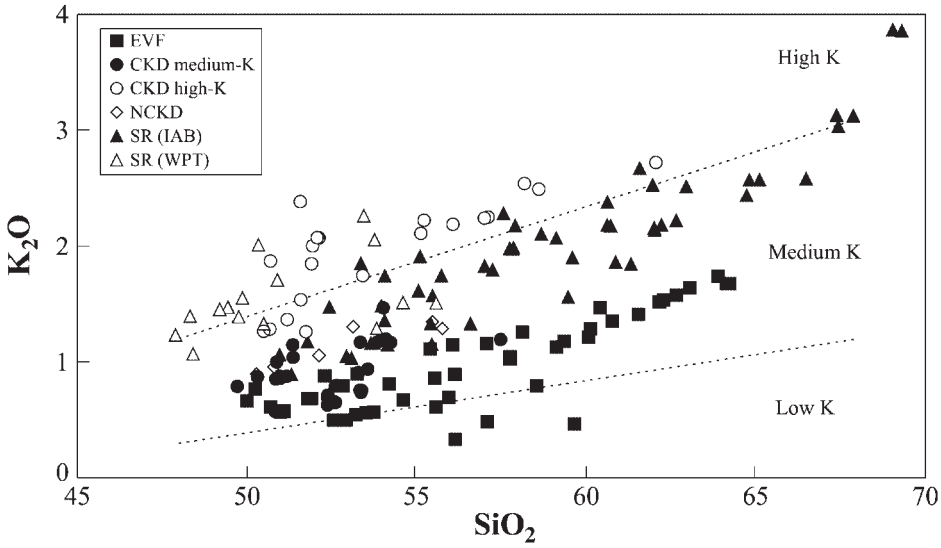

Fig. 2. K_2O (wt %) vs SiO_2 (wt %) for volcanic rocks along an east–west transect across the northern Kamchatka Peninsula. Some high-K rocks occur in the Central Kamchatka Depression (CKD), which are marked by open circles. Mafic within-plate type rocks (WPT) of Ichinsky from the Sredinny Ridge (SR) also plot in the high-K field. EVF, Eastern Volcanic Front; IAB, island-arc basalt type rocks; classification lines after Le Maitre *et al.* (1989).

Trace element patterns for EVF, CKD and SR rocks with >5% MgO have typical arc signatures with strong but variable LILE and LREE enrichment and low HFSE (Fig. 3). Exceptions are the few monogenetic cones around the back-arc Ichinsky volcano (see below). LILE and HFSE concentrations increase across the arc from front to back. CKD and EVF rocks are depleted in Nb and Ta and REE compared with N-MORB. HREE are much lower than in N-MORB and change only slightly between the three groups. WPT rocks at Ichinsky are more enriched in LILE and LREE than the IAB of the SR, and have rather high HFSE concentrations. The Nb–Ta depletions in back-arc rocks compared with neighbouring LILE are therefore much smaller than in the IAB.

Fractionation correction

Mafic samples in the EVF, CKD and SR have MgO contents up to 8·5%, 12·3% and 9·2%, respectively. The *mg*-number ranges from 0·26 to 0·71, thus some samples are close to primary mantle-derived melt compositions whereas others are not. Direct comparison of trace element concentrations is therefore impossible. To minimize the effects of fractional crystallization on trace elements, it is necessary to correct the data to a common magma composition. We choose a recalculation procedure (see below), to evaluate the complete trace element patterns of source(s) and fluid compositions. We also use incompatible element ratios of elements of equal partition coefficient.

For correction we choose the approach used by Plank & Langmuir (1988). Analyses of each volcano were plotted on MgO variation diagrams, which show the individual trends for the centres we sampled. Examples of such trends are given in Fig. 4. Regression lines are drawn through the data and the intercept of the trend line at 6% MgO gives the fractionation-corrected values for major and trace elements. This approach assumes a constant fractionation assemblage. Different olivine/clinopyroxene ratios will cause deviation in the trends because olivine is more Mg rich than clinopyroxene (cpx) and thus the melt will be more strongly depleted in MgO than for cpx-dominated fractionation. Such differences, however, are small. Ratios of incompatible trace elements, however, should not change. Plagioclase fractionation starts at ~5% MgO, as seen in distinct kinks in major element trends (Fig. 4). Magnetite fractionation starts at different MgO contents and is responsible for Fe (and Ti) depletion in more evolved rocks (Fig. 4). Therefore we have used only samples with >5% MgO to calculate the regression lines and normalized concentrations.

K_2O/Na_2O should not change during early ol–cpx fractionation and the regression lines should give subhorizontal lines in plots of MgO vs K_2O/Na_2O. This is the case for most of our sample suites. However, samples from two CKD volcanoes, Tolbachik and Ploskie Sopky, show a second trend of increasing K_2O/Na_2O with fractionation. This trend is probably related to crustal processes and these samples are excluded from the discussion of across-arc source differences. Also, the NCKD volcanoes and the WBT rocks at Ichinsky volcano are

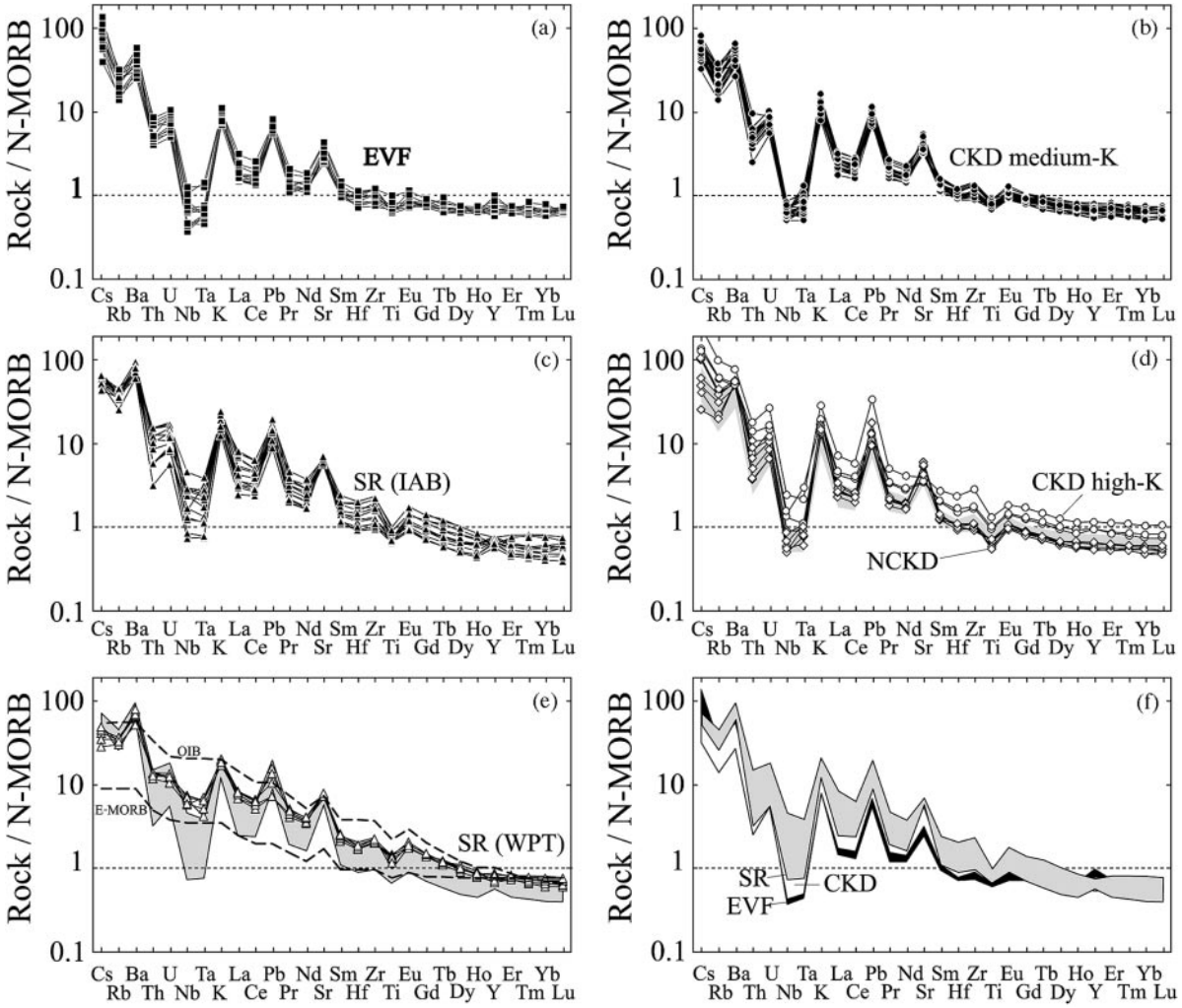

Fig. 3. N-MORB-normalized trace element patterns for mafic rocks with >5% MgO for the various regions of the North Kamchatka transect. The order of incompatible elements is derived from Hofmann (1988) with Cs and all REE added. N-MORB values after Sun & McDonough (1989). Same symbols as in Fig. 2. (a–c) Trace element distributions in the EVF, CKD and SR. (d) High-K rocks of the CKD and lavas from NCKD compared with typical island-arc basalts of the CKD (shown by the shaded field). (e) Within-plate type (WPT) rocks compared with the 'normal' island-arc rocks of the SR (grey field), and E-MORB and OIB compositions after Sun & McDonough (1989). (f) Comparison of the pattern of typical arc basalts from each zone. For clarity, each zone is expressed by a compositional field.

discussed separately. Errors of the calculated values were estimated by Student's *t*-test for populations with <20 data points. The recalculated values are marked by a 6·0 subscript and plotted with error bars in Figs 5–7 against slab depth.

For some volcanoes we only have a few samples with >5% MgO. For the Ploskie Sopky, Shiveluch, Zarechny and Kharchinsky volcanoes and the IAB series of Ichinsky volcano our data are combined with the data of O. Volynets (deceased, unpublished data, available on request) and literature data. Fewer than five samples with >5% MgO were available for Kamen (two), Gamchen (four), Achtang (three) and Shmidt (two). For these samples the statistical errors were not calculated. No rocks with >5% MgO exist for Nikolka volcano, which was not used for extrapolation. Incompatible trace elements are well correlated with MgO; the relative deviation from the regression line in the range >5% MgO is ~10–20%.

Across-arc major and trace element variations

The $(MgO)_{6\cdot0}$ corrected concentrations were combined with subduction zone parameters such as crustal thickness, distance to the trench and the depth to the slab surface. Plank & Langmuir (1988) and Pearce & Parkinson

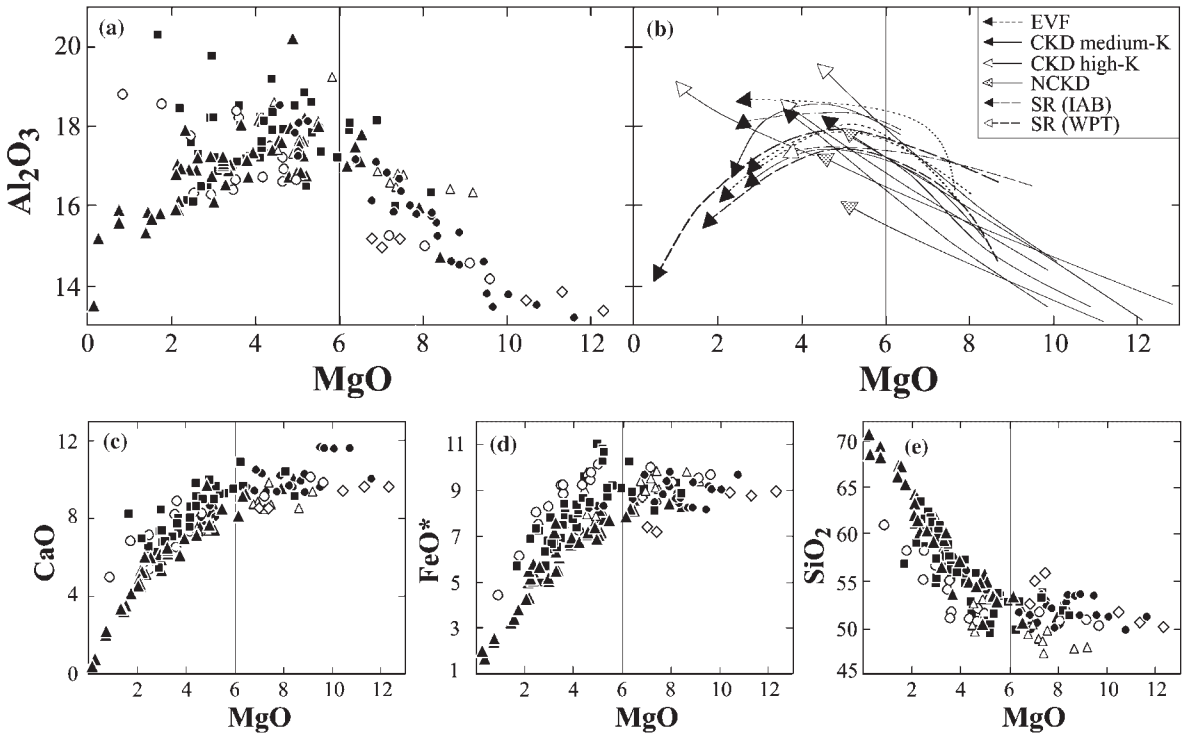

Fig. 4. (a) MgO vs Al_2O_3, reflecting the beginning of plagioclase fractionation, which results in a decrease in Al_2O_3. Some outliers to higher Al_2O_3 are probably altered by plagioclase accumulation. For rocks with MgO >5% plagioclase fractionation can be regarded as negligible. (b) Fractionation trends of single volcanoes, defined by arrows. The EVF, CKD and SR are marked by dotted, continuous and dashed lines, respectively. (c–e) MgO vs CaO, FeO* and SiO_2 diagrams for all sampled suites. Same symbols as in Fig. 2. Element concentrations are given in wt %.

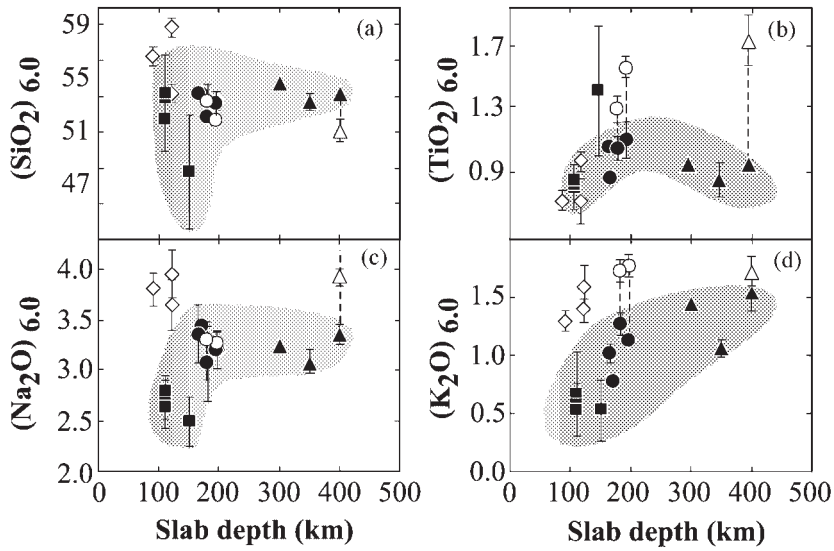

Fig. 5. (a–d) The 6% MgO normalized major element concentrations for single volcanoes plotted relative to the depth of the slab surface below the volcano. The typical arc series of Tolbachik, Ploskie Sopky and Ichinsky are connected by a dotted line with the high-K series and WPT, respectively, occurring at the same volcano. The shaded fields were drawn to underline the trends of the typical arc magmas. Symbols as in Fig. 2. Element concentrations are given in wt %.

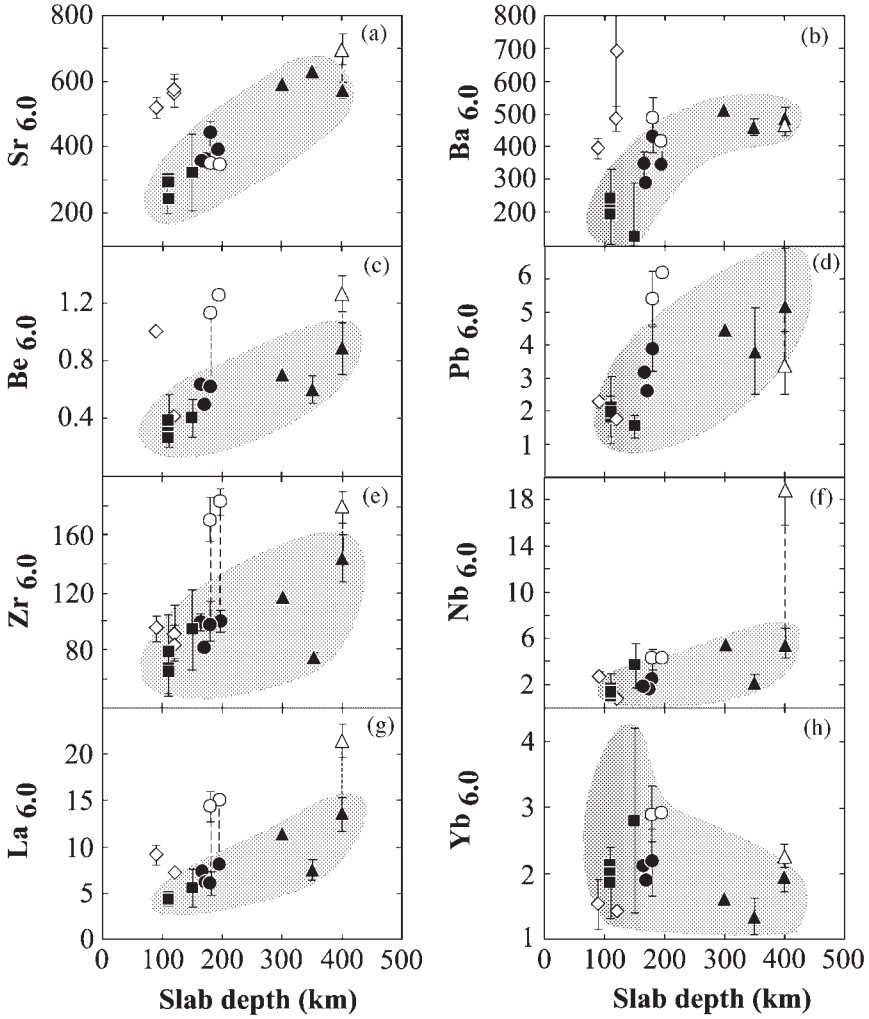

Fig. 6. The 6% MgO normalized fluid mobile trace element concentrations (a–d) and HFSE and REE concentrations (e–h) of single volcanoes plotted relative to the depth of the slab surface below the volcano. Symbols as in Fig. 2. Element concentrations are given in ppm.

(1993) have suggested that the extent of melting may depend on the height of an upwelling melting column, which, in turn, they assumed to be controlled by subduction geometry. Minor variations in crustal thickness from 30 to 40 km, however, are insufficient to generate the observed large trace element variations simply by different degrees of melting.

Trench distance and depth to the slab surface are directly related. The worldwide similar position of the frontal volcanic zone at ~110–130 km above the slab surface indicates that melting is caused by slab fluids, which were liberated mostly by temperature-sensitive dehydration reactions (see Tatsumi & Eggins, 1995; Schmidt & Poli, 1998; and therein). Therefore we prefer the depth of the slab surface below the volcano (after Gorbatov, 1997) as a reference for regional variations.

The data are shown for selected major and trace elements and element ratios vs depth of the slab surface in Figs 5–7. The high-K calc-alkaline and within-plate rocks, as well as the NCKD group, are marked in the diagrams and will be discussed separately. Most $(MgO)_{6·0}$ normalized incompatible trace elements, i.e. HFSE (Zr, Nb, also Hf and Ta; not shown), LILE (Sr, Ba, Rb, Be, Pb, U, Th), LREE, some major elements (K, Na) and certain element ratios (K/Na, La/Yb, Sr/Y, Nb/Yb) increase with slab depth. The strongest increase, by more than two times from front to back-arc, is observed for K_2O, Ba, Sr and Rb. A slightly different behaviour is found for Na_2O, the LREE and HFSE, which all strongly increase from the EVF to the CKD but show a much weaker increase further to the SR. Ti shows a similar behaviour and is even depleted in the SR compared with the CKD. No correlations at all exist for Y and the HREE, which are almost constant from front to back-arc. The rocks of the CKD show comparably large scatter in incompatible

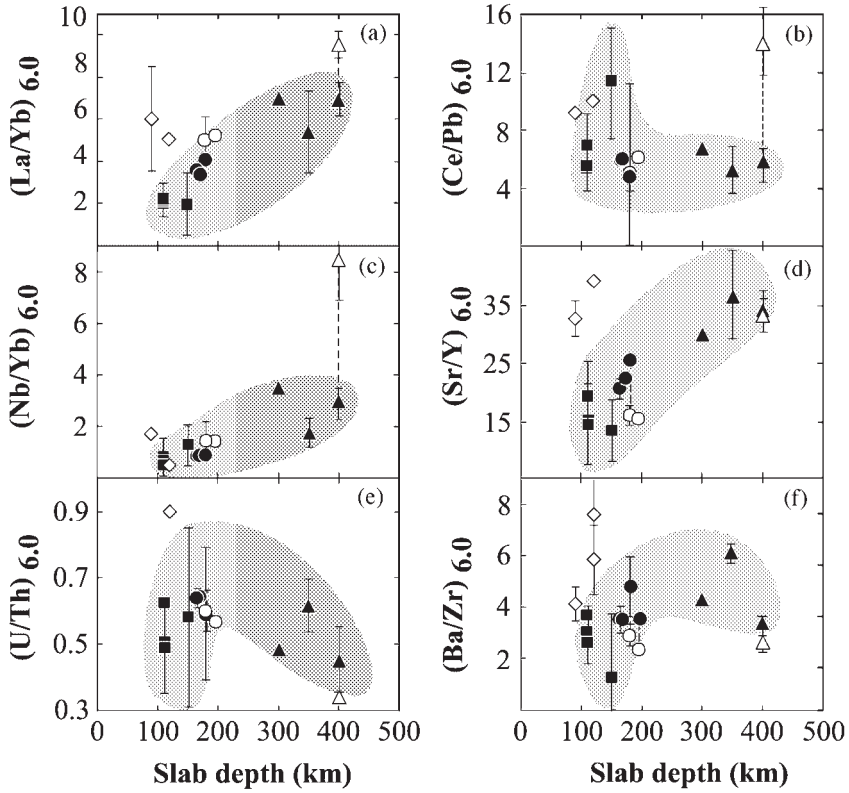

Fig. 7. (a–f) The 6% MgO-normalized incompatible trace element ratios of single volcanoes plotted relative to the depth of the slab surface below the volcano. Positive linear trends exist for $(La/Yb)_{6\cdot0}$, $(Nb/Yb)_{6\cdot0}$ and $(Sr/Y)_{6\cdot0}$. The $(Ce/Pb)_{6\cdot0}$, $(Ba/Zr)_{6\cdot0}$ and $(U/Th)_{6\cdot0}$ ratios do not show regular trends. Symbols as in Fig. 2.

elements. Variations among high-K calc-alkaline and NCKD rocks are even larger.

Compatible major (Si, Fe, Ca), minor and trace elements (P, Ni, Co, V, Sc) are highly sensitive to fractionation and thus difficult to normalize to a certain MgO content. These elements will therefore not be considered further in reconstruction of elemental variations in primary magmas and their mantle sources.

Our results for the across-arc trends in incompatible elements are comparable with those obtained from other arcs such as the Kurile Islands (Avdeiko *et al.*, 1991) and Japan (Shibata & Nakamura, 1997).

The high-K calc-alkaline rocks, rocks of the NCKD and the WPT of the SR deviate in some elements from the trends. The high-K calc-alkaline basalts of Tolbachik and Ploskie Sopky volcanoes are strongly enriched in K_2O, TiO_2, P_2O_5, Rb, Ba, Be, HFSE (Zr, Nb, Ta, Hf), Y and REE compared with the 'normal' rocks of the CKD. The rocks of the NCKD are enriched in SiO_2, Na_2O, K_2O, Ba, Sr, Rb, Pb, Th, U and LREE, and depleted in the HREE and Y compared with volcanic centres of the EVF and, for most elements, also compared with the CKD. NCKD rocks have the highest Sr/Y and La/Yb ratios for Quaternary rocks of Kamchatka. HFSE are similar in concentrations to typical CKD rocks. The WPT at Ichinsky have higher concentrations of Na_2O, TiO_2, P_2O_5, Sr and all HFSE and REE, and are depleted in SiO_2 and Rb compared with the Ichinsky IAB. The HFSE and LREE concentrations are much higher than in all other studied rocks. Consequently, they have high Ce/Pb and La/Yb, and low U/Th and Ba/Nb ratios.

The U/Th ratios of all Kamchatka rocks are higher than those in N-MORB and generally are in the range of 0·41–0·58, 0·57–0·71 and 0·38–0·64 for the EVF, CKD and SR, respectively. One remarkable outlier in the CKD is sample 2310 from Kamen volcano with a U/Th ratio of 0·79, the highest ratio found in any primitive basalt of Kamchatka. This large ratio is coupled with the lowest content in all LILE and LREE and highest in HREE within the CKD suite.

Sr, Nd and Pb isotopes

Isotope data for the transect are summarized in Table 2 and Fig. 8. The data plot close to the MORB field and variations in all isotope systems are small and inside the previously reported ranges for Kamchatka (Kersting &

Arculus, 1995; Tatsumi *et al.*, 1995; Kepezhinskas *et al.*, 1997; Turner *et al.*, 1998). From the more extensive and representative sampling, we can, however, identify within the Kamchatka field a fine-scale structure for the regions and in some cases even single volcanoes. There is a general increase in $^{87}Sr/^{86}Sr$ and $^{143}Nd/^{144}Nd$ from the EVF to the CKD and a decrease from the CKD to the SR (Figs 8 and 9). The fields of the EVF and SR are nearly identical in Sr–Nd-isotope space, except for two samples from Komarov volcano with slightly higher Sr-isotope ratios. A larger range exists in Nd isotopes for the EVF and SR compared with the relatively narrow range in Sr isotopes. Within-plate type rocks of the back-arc (SR WPT rocks) have lower $^{143}Nd/^{144}Nd$ ratios than all other samples including 'normal' SR IAB rocks. WPT rocks are also relatively radiogenic in Sr. The highest $^{87}Sr/^{86}Sr$ ratio is found in the CKD Kluchevskoy lavas ($^{87}Sr/^{86}Sr = 0{\cdot}70366$). High-K calc-alkaline basalts and the high-Mg andesites of the NCKD are on average lower in Sr- and similar in Nd-isotopic ratios compared with the other CKD rocks.

In Pb isotopes, the CKD lavas are less radiogenic compared with the EVF, but similar to the SR rocks (Fig. 8). The high-K calc-alkaline basalts are significantly displaced to unradiogenic Pb-isotopic compositions. The Shiveluch sample from the NCKD has Pb ratios comparable with those for the CKD rocks. Also, the WPT rocks are identical in Pb isotopes to the other rocks of the SR. The data for the Bakening volcano (EVF, 200 km to the south of the transect, after Dorendorf *et al.*, 2000b), and xenolith data (Dorendorf *et al.*, 1999, unpublished) are given for comparison in Fig. 9. Bakening lavas are even more unradiogenic in Sr at comparable Nd- and Pb-isotopic ratios. The field of leached clinopyroxene from mantle xenoliths for Kamchatka shows for Nd isotopes a comparable (except for one sample with higher ratio) and for Sr isotopes a larger range from depleted to enriched than that observed in the volcanic rocks (Fig. 9).

INTERPRETATION

Geochemical zonation across Kamchatka and possible causes

A significant geochemical zonation across the arc was shown for major and trace elements from the EVF over the CKD to the SR (Figs 5–7). By using only data restricted to MgO-normalized values and incompatible element ratios rather than absolute element concentrations of basaltic rocks (>5% MgO) we can minimize different degrees of magmatic differentiation as a possible cause. Other causes for these variations then are: (1) different mantle sources; (2) slab-derived hydrous fluid enrichment; (3) contribution of water-rich melts or (4) bulk sediments from the slab; (5) decreasing degrees of melting at increasing pressures and reduced fluid flux from the slab further away from the arc front.

Using Pb- and Be-isotope data, Kersting & Arculus (1995) and Tsvetkov *et al.* (1989) argued that subducted sediments play a minor role in magma generation in Kamchatka volcanic rocks. Additionally, it was shown by the variation in Sr- and O-isotope data that the fluid is largely derived from the altered oceanic crust (Dorendorf *et al.*, 2000a), rather than sediments.

Melting process

Decreasing melting degrees of a mantle source composed of olivine, orthopyroxene and clinopyroxene will result in enriched incompatible elements in the melt. Only for very low melting degrees (<5%), which are not appropriate for most island-arc lavas (Plank & Langmuir, 1993), may highly incompatible elements be fractionated from each other. Low degree of melting could be assumed for only the back-arc WPT rocks (see below). Residual garnet in the mantle can also strongly influence HREE and Y because it buffers these elements in the melt at a low level until it is completely consumed. Because REE patterns are flat on N-MORB-normalized diagrams, the La/Yb ratio is relatively low for all rocks, ranging from 1·83 to 10·28. HREE concentrations are only 6–15 times the chondritic values. It is therefore not likely that residual garnet was prominent in the mantle sources of Kamchatka volcanic rocks.

Plank & Langmuir (1988) have argued that the distance between the upper plate and slab surface below the active volcanic front in arcs worldwide is directly linked with the height of the melting column. This is expressed in a negative correlation between $Ca_{6\cdot0}$ and $Na_{6\cdot0}$ and crustal thickness. The reason for such a trend is that Ca is retained by clinopyroxene in the mantle residue and Na is not. Our data, when plotted on a $(CaO)_{6\cdot0}$ vs $(Na_2O)_{6\cdot0}$ diagram, fall on the Plank & Langmuir (1988) trend of decreasing $(CaO)_{6\cdot0}$ and increasing $(Na_2O)_{6\cdot0}$ with slab depth (Fig. 10a). $(Na_2O/CaO)_6$ increases rapidly from EVF to CKD and then remains constant to the SR (Fig. 10b). The highest $Na_{6\cdot0}$ values are from the WPT basalts and rocks from the NCKD. This would favour comparably low melting degrees in these rocks. EVF rocks have the highest degree of melting (20%) using Plank & Langmuir (1988). For the CKD and SR 'normal' arc rocks and high-K calc-alkaline basalts with lower degrees of melting (9–12%) the spread is limited and not related to the depth of the slab (Fig. 10a). This result is surprising because the degrees of melting do not correlate with slab depth. This can be explained if the melting process is governed by two stages (Pearce & Parkinson, 1993). The first melting stage results from fluid flux into the mantle.

Table 2: Sr-, Nd-, and Pb-isotope composition of selected rocks of the transect

	$^{87}Sr/^{86}Sr$	±2 SE	$^{143}Nd/^{144}Nd$	±2 SE	$^{206}Pb/^{204}Pb$	$^{207}Pb/^{204}Pb$	$^{208}Pb/^{204}Pb$
EVF							
GAM-12	0·703401	±13	0·512991	±4	18·316	15·508	38·138
GAM-28	0·703346	±14	0·513033	±6	18·335	15·510	38·070
SHM-01	0·703344	±13	0·513070	±6	18·306	15·495	37·960
SHM-04	0·703383	±14	0·513032	±4			
KOM-02	0·703482	±11	0·513036	±7			
KOM-06	0·703386	±14	0·513044	±5	18·343	15·528	38·159
KOM-11	0·703605	±14	0·512977	±5			
KIZ-01/1	0·703352	±11	0·513045	±5			
KIZ-24	0·703347	±15	0·513048	±5			
KIZ-24/1	0·703370	±11	0·513047	±5	18·320	15·502	38·033
CKD							
2330	0·703379	±12	0·513078	±6	18·242	15·474	37·885
3-90	0·703399	±15	0·513069	±6	18·267	15·508	38·015
5-90	0·703430	±13	0·513081	±5			
PLO-16	0·703605	±10	0·513104	±6			
2310	0·703466	±13	0·513115	±7	18·292	15·478	37·885
22-8	0·703331	±13	0·513106	±14			
655	0·703368		0·513077	±6			
201	0·703341	±12	0·513095	±6	18·192	15·482	37·885
TOL-03	0·703356	±13	0·513081	±5	18·185	15·472	37·850
TOL-06	0·703344	±08	0·513084	±5	18·154	15·421	37·698
8883	0·703441	±10	0·513097	±6			
KLU-03	0·703585	±17	0·513080	±6	18·281	15·500	37·971
KLU-04	0·703543	±11	0·513068	±7	18·285	15·498	37·970
KLU-06	0·703605	±08	0·513070	±6			
KLU-07	0·703541	±15	0·513085	±6	18·297	15·496	37·972
KLU-08	0·703534	±12	0·513095	±6	18·295	15·517	38·010
KLU-09	0·703527	±14	0·513096	±5			
KLU-10	0·703524	±12	0·513121	±6	18·292	15·514	37·999
KLU-11	0·703499	±13	0·513111	±6	18·287	15·505	37·974
KLU-12	0·703664	±14	0·513102	±6	18·303	15·509	37·997
KLU-13	0·703665	±13	0·513094	±5			
KLU-14	0·703634	±13	0·513089	±5			
KLU-15	0·703509	±16	0·513109	±7	18·300	15·489	37·941
KLU-16	0·703536	±12	0·513098	±6	18·309	15·498	37·973
2569	0·703370	±11	0·513114	±8			
2585	0·703389	±17	0·513124	±6	18·357	15·483	37·918
8837	0·703450		0·513097	±6			
90093	0·703472	±17	0·513112	±5			
SR							
ESO-04	0·703342	±10	0·513063	±6			
ESO-08	0·703355	±13	0·513092	±6	18·249	15·486	37·916
ACH-02	0·703352	±14	0·513044	±6			
ACH-03	0·703295	±13	0·513032	±6			
6250	0·703344	±13	0·513077	±5			
6283	0·703352	±16	0·513035	±6			
6334/1	0·703353		0·513053	±5			
ICH-02	0·703379	±10	0·513046	±7			
ICH-05	0·703395	±17	0·512987	±5	18·057	15·476	37·952
ICH-07	0·703391	±13	0·512997	±6			
ICH-10	0·703405	±13	0·512974	±6			
ICH-19	0·703329	±14	0·513054	±5	18·248	15·497	37·953
ICH-31	0·703364	±12	0·513041	±5	18·248	15·488	37·975
ICH-32	0·703397	±14	0·513004	±7			
ICH-49	0·703368	±15	0·513049	±6			
ICH-64	0·703319	±12	0·513044	±6			

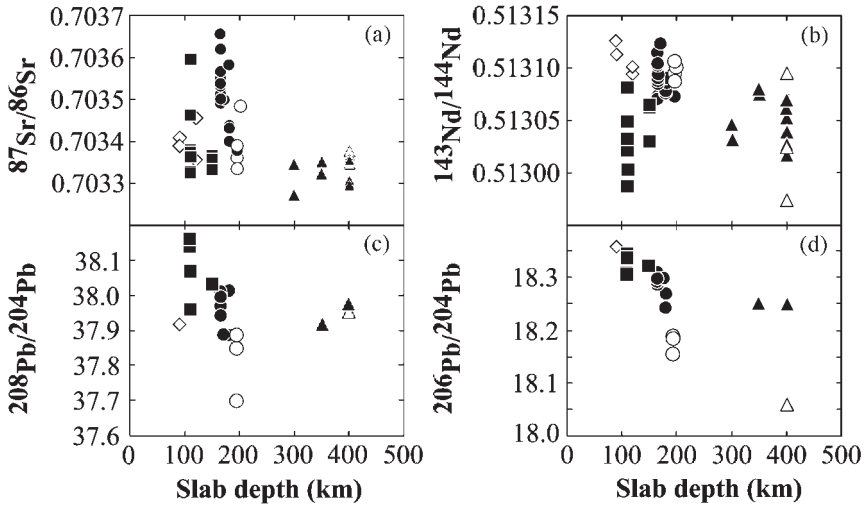

Fig. 8. (a–d) Variation of Sr, Nd and Pb isotopic ratios plotted relative to the depth of the slab surface. Symbols as in Fig. 2.

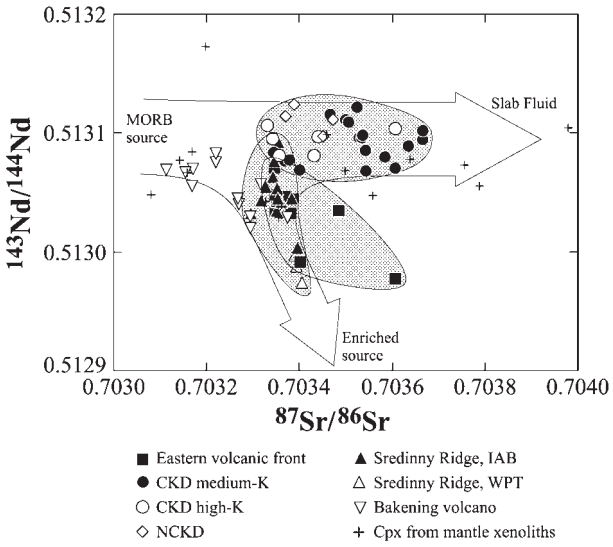

Fig. 9. $^{143}Nd/^{144}Nd$ vs $^{87}Sr/^{86}Sr$ for the volcanic rocks of Kamchatka. The arrows are drawn schematically to show the three-component mixing between MORB, slab fluid and OIB-source mantle. Symbols as in Fig. 2. Also plotted are data for leached Cpx from mantle xenoliths (+) (unpublished data) and for the Quaternary Bakening volcano (▽), 200 km to the south of the west–east transect (Dorendorf *et al.*, 2001).

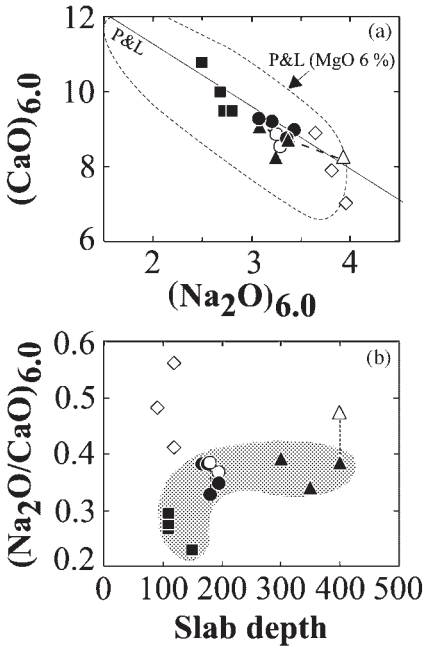

Fig. 10. (a) $(CaO)_{6\cdot0}$ vs $(Na_2O)_{6\cdot0}$ as used by Plank & Langmuir (1988) to estimate the melting degree for volcanic front lavas. The field for the 6% MgO normalized data of Plank & Langmuir (1988) (P&L) is compared with our data. There exists a similar but less extended variation for the whole dataset from Kamchatka. However, the variation is limited from 10% to 20% of melting if only the typical arc magmas (black symbols) are regarded. (b) $(Na_2O/CaO)_{6\cdot0}$ vs depth of the slab surface below the volcano. The typical arc series of Tolbachik, Ploskie Sopky and Ichinsky are connected by a dotted line with the high-K series and WPT, respectively, occurring at the same volcano. The shaded field emphasizes the trends of the typical arc magmas. $(Na_2O/CaO)_{6\cdot0}$ is not related to the depth of the slab surface, increasing rapidly from EVF to CKD and then remaining constant to the SR. Symbols as in Fig. 2.

A second stage of melting results from mantle upwelling and decompression.

Mantle source variations before fluid addition

The nature of the mantle source is expressed by the slope of the immobile trace element in normalized trace element variation diagrams. This pattern is not changed significantly by moderate to large degrees of melting,

and thus source patterns can be inferred from the melt [compare, e.g. OIB (ocean-island basalt) in Fig. 3e]. HFSE and HREE are assumed to have relatively low concentrations in the slab fluid (Brenan *et al.*, 1995; Ayers *et al.*, 1997; Stalder *et al.*, 1998). Thus, for these elements the mantle contribution is much greater than the slab contribution. Pearce & Parkinson (1993) showed that, using relationships between different groups of these elements (very highly incompatible, VHI; highly incompatible, HI; moderately incompatible, MI), it is possible to estimate the degree of depletion or enrichment and hence the overall trace element patterns of the source before fluid addition. Melting models for the fertile MORB mantle (FMM) show that even a slight depletion (e.g. after 5% of melt lost) will immediately be reflected in the depletion of the VHI elements (Pearce & Parkinson, 1993). Hence, different degrees of melting of the FMM source will produce melts with VHI = HI = MI for large degree of melting and VHI > HI > MI for small degree of melting.

Normalized trace element variation diagrams with our data normalized to fertile MORB mantle (FMM) are shown in Fig. 11. It is clear that Kamchatka mantle sources are depleted but only slightly more so than for MORB. A smooth line drawn through HREE and HFSE shows only very weak depletions relative to N-MORB (Fig. 3). Following Pearce & Parkinson (1993) we can estimate in more detail the type of source and degrees of melting. EVF and CKD calc-alkaline rocks have patterns of VHI $\geq$ HI = MI, which correspond to higher degrees of melting (15–20%) of MORB mantle, in accordance with our estimations from $(CaO)_{6{\cdot}0}$–$(Na_2O)_{6{\cdot}0}$ systematics. The pattern for CKD high-alkaline rocks (VHI > HI > MI) corresponds to moderate degrees of melting (<15%) of MORB mantle. Rocks of the SR (IAB) with VHI$\gg$HI $\geq$ MI show a pattern of high degree of melting of a slightly enriched source. WPT lavas (VHI $\gg$ HI > MI) match the pattern for low to moderate degrees of melting of enriched FMM (Fig. 11).

This result is confirmed by Nb/Yb ratios (Fig. 7c), which show that the sources of the EVF and CKD magmas are similar to a MORB source. By contrast, the SR magmas have slightly higher Nb and Nb/Yb ratios, especially for the WPT of Ichinsky. This cannot be the effect of garnet, which depletes Yb compared with Nb; furthermore, a similar behaviour is found for the Nb/Zr ratios. This means that an enriched mantle component exists below the back-arc.

The variation of Th/Yb vs Ta/Yb was used by Pearce (1983) to distinguish between primitive island-arc rocks from depleted sources and enriched sources (Fig. 12). The displacement from the mantle field to higher Th/Yb ratios is caused by enrichment in Th over Yb (from fluid or sediment), whereas variation in the mantle source is shown by a change in both ratios. If Th over Yb enrichment reflects a sediment contribution, then Pb isotopes should be just as sensitive to a sediment contribution as Th. These, however, do not show involvement of sediments (Kersting & Arculus, 1995). Therefore, the variable displacement of the data above the mantle array is attributed here to enrichment by fluids (Dorendorf *et al.*, 2000). SR rocks form an array towards an enriched mantle component. Overall, the observed trend suggests more or less slab component added to a depleted to slightly enriched mantle source. The mass balance of this mixing process is outlined below.

The enriched component: deep fluids, subducted sediments or OIB source?

We need to consider three alternative explanations for the observed HFSE enrichment in the back-arc: an OIB component, subducted sediments or deep fluids in the mantle wedge. Below the SR, fluids are liberated at higher temperatures and pressures from the slab, i.e. conditions where HFSE-retaining phases may no longer be stable in the slab. Additionally, high-P–T fluids have larger solute contents, which enhance their capability to transport HFSE (Brenan *et al.*, 1995; Bureau & Keppler, 1999). The fluid calculated by Stolper & Newman (1994) for the enrichment in back-arc basalts is relatively enriched in Y but has a Ta/Y ratio only twice that of the N-MORB source. We can predict this also for the Nb/Yb ratio because Nb and Yb behave similarly to Ta and Y in the mantle. It is therefore difficult to explain Nb/Yb ratios in the WPT of Ichinsky, which are about 10 times enriched over N-MORB by such fluids.

Different sources should also be detectable in isotope ratios. Figure 9 shows an isotope compositional field where the data for volcanic rocks from Kamchatka are distributed in three directions, suggesting involvement of three components. The component low in $^{87}Sr/^{86}Sr$ (<0·7031) and high in $^{143}Nd/^{144}Nd$ ($\sim$0·5131) is the MORB source within the mantle wedge. From the MORB field, one array trends to higher Sr-isotope ratios with unchanged Nd-isotope ratios. Slab fluids are expected to have such a composition but sediments are not. The second array begins from a point on the first trend (i.e. a fluid-enriched MORB composition) and trends to lower Nd-isotope ratios with a correlated increase in $^{87}Sr/^{86}Sr$. Such a trend probably results from mixing with an enriched mantle component. This trend is formed mainly by the SR back-arc rocks, which supports the interpretation that some enriched component such as OIB source mantle exists in their source. Volynets *et al.* (1997*a*) argued on the basis of Sr- and Nd-isotope compositions of Miocene WPT rocks from East Kamchatka that they contain such an EM1 component (Zindler & Hart, 1986).

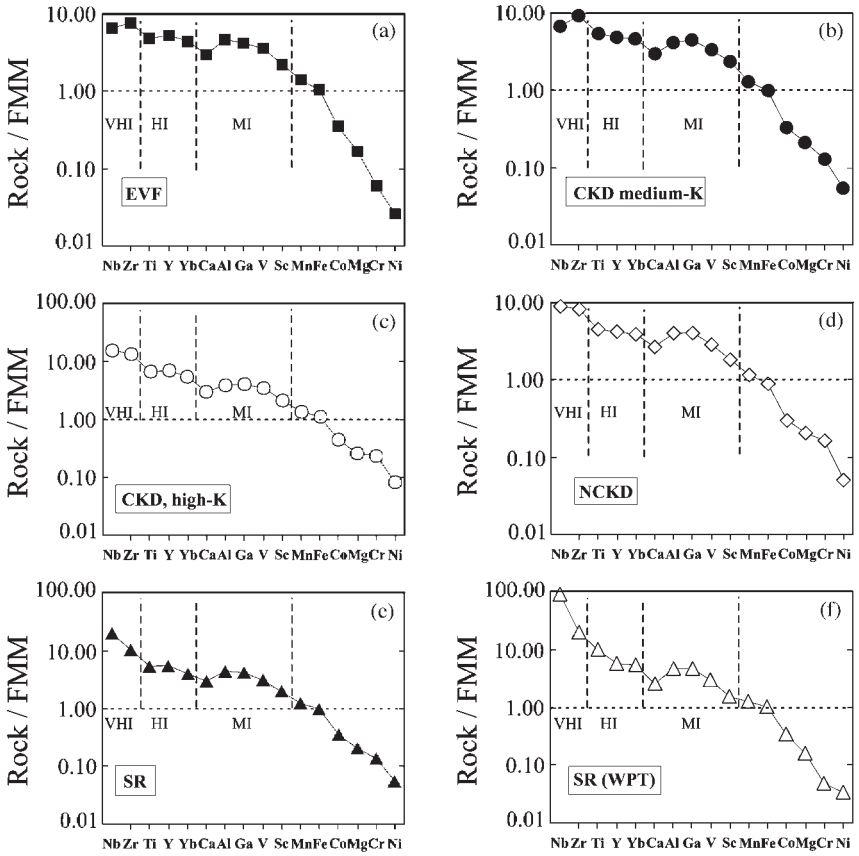

Fig. 11. Patterns of mainly mantle-derived elements normalized to fertile MORB mantle (FMM) after Pearce & Parkinson (1993) for the volcanic suites of Kamchatka, showing a range of variation as a result of melting and depletion–enrichment events in the mantle. Dashed lines distinguish the very highly incompatible (VHI: Nb and Zr), highly incompatible (HI: Ti, Y, Yb) and moderately incompatible (MI: Ca, Al, Ga, V, Sc) elements. Symbols as in Fig. 2.

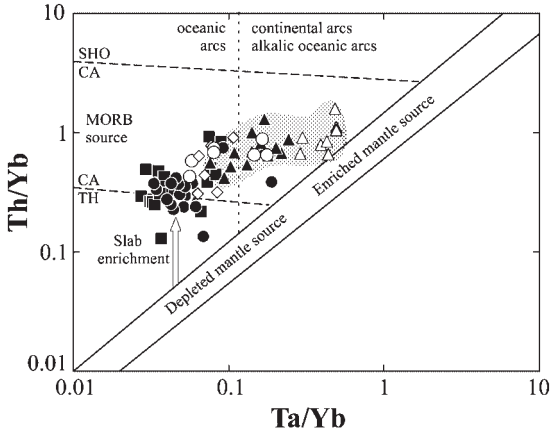

Fig. 12. Th/Yb vs Ta/Yb after Pearce (1983). Nearly all samples from the CKD and EVF fall into the field of oceanic arcs formed from depleted mantle sources. In contrast, the SR samples trend towards an enriched mantle composition (shaded field). High-K rocks and the samples from the NCKD have compositions slightly enriched in Th and Ta. SHO, shoshonitic series; CA, calk-alkaline series; TH, tholeiitic series. Symbols as in Fig. 2.

From the low Pb-isotope ratios in SR rocks we can rule out terrigenous Pacific sediments in their mantle source. Sediments from the Emperor Seamounts chain, however, could have caused enrichment in trace elements. If such sediments are subducted below Kamchatka together with the Emperor Seamounts chain, they must influence EVF and CKD rocks as well, which is not observed.

The EVF rocks form a rather large field between the two trends. Low HFSE values in the EVF rocks argue against an OIB-source component for these volcanic rocks. Decreasing $^{143}Nd/^{144}Nd$ are coupled with higher Pb-isotope ratios (Fig. 8c) and enrichment in Th/Nb. Kersting & Arculus (1995) showed that Pacific sediments from the latitude of Kluchevskaya Group are higher in Pb isotope ratios and lower in $^{143}Nd/^{144}Nd$, and could influence the magmatic source below Kamchatka. On the basis of high $^{208}Pb/^{204}Pb$ coupled with low $^{143}Nd/^{144}Nd$ and HFSE, a minor sediment component is seen in some EVF lavas only.

We conclude that the mantle source below Kamchatka is similar to N-MORB mantle, but slightly more depleted,

with a contribution of an OIB-source component in the back-arc region.

Variations in the amount and composition of the slab fluid

The Ce/Pb ratio reflects the degree of fluid enrichment, as Pb is highly mobile in slab fluids but behaves similarly to Ce in melting and crystallization processes (Miller *et al.*, 1994). In all three regions Ce/Pb is ~5–7 and there is no systematic change in that ratio in relation to the depth of the slab surface. Kizimen volcano of the EVF and the WPT of the SR deviate to higher Ce/Pb ratios. Considering the La and Pb variations (Fig. 6g and d, respectively), it is obvious that this deviation is caused by the lower Pb content, suggesting lower fluid input for the latter.

The constant ratios of Ba/Zr (Fig. 7d) and Ba/La (not shown) indicate that the degree of fluid enrichment for Ba does not significantly change from the frontal zone to the back-arc. However, Ba, LREE and HFSE concentrations are also influenced by mantle wedge depletion or enrichment (see above). Radiogenic isotope variations can partly clarify this question. If the slab fluid differs in Sr- and Pb-isotopic ratios from the mantle (which can be assumed at least for Sr from the altered oceanic crust), a high proposed concentration of these elements in the fluids will influence the isotope ratios in the fluid-metasomatized mantle. Pb isotopic ratios decrease from the frontal zone to the CKD and remain constant towards the back-arc (Fig. 8c and d). Limited and decreasing amounts (<1%) of sediment in the source of the frontal lavas could cause this trend. Sr- and Nd-isotopic ratios are not so sensitive because of relatively higher concentrations of these elements in the mantle wedge. Therefore, Sr isotopes behave differently from Pb isotopes: $^{87}Sr/^{86}Sr$ isotopic ratios increase from the EVF to the CKD and then decrease strongly to the SR (Fig. 8a). This shows that the CKD source is distinct but that this difference is not necessarily related to a recent fluid influx. The higher U/Th ratios in CKD rocks could be explained by fluid enrichment or by different source composition before fluid-induced melting. U–Th isotope data are close to the equiline for most rocks from Kamchatka (Dorendorf, 1998; Turner *et al.*, 1998). A subset of samples from Kluchevskoy volcano suggests an isochron relation giving ~130 ka since U/Th fractionation (Dorendorf *et al.*, 1999, unpublished data). In any case, the enrichment is not recent and not related to the process of melting.

Assessing across-arc variations in fluid flux is complicated by the fact that the slab fluid composition could change depending on the extent of dehydration and type of residual minerals in the slab (Bureau & Keppler, 1999). Different models describe the mineral composition and dehydration of the subducting slab (Tatsumi & Eggins, 1995; Schmidt & Poli, 1998). With our data we can test whether the pressure- and temperature-dependent dehydration of certain phases such as amphibole, phengite or lawsonite are in fact reflected in a changing fluid composition.

The high concentrations of Rb, K, Ba and Sr in arc magmas can be an indication that amphibole has retained these elements until it breaks down at >60–70 km depth. The dehydration of phengite should be reflected by a strong flux of Rb into the mantle, which should be detectable by a decreasing K/Rb ratio (Melzer & Wunder, 2000). This ratio is variable in mafic rocks of the EVF (300–600) and CKD (400–600) but relatively constant in the IAB of the SR (460–520). The high-K calc-alkaline rocks have slightly lower (320–340) and the WPT (~600) slightly higher K/Rb ratios. The phengite effect therefore cannot be demonstrated here, in contrast to findings by Tatsumi *et al.* (1995) and predictions made by Melzer & Wunder (2000).

Increasing La/Yb from the frontal zone to the back-arc is a result of increasing La at constant Yb concentrations (Fig. 13). Because no garnet signatures in Kamchatka mantle sources were observed, this strong increase from front to back-arc in LREE could be explained by dehydration of lawsonite, which strongly concentrates the LREE (Tribuzio *et al.*, 1996; Bureau & Keppler, 1999) and is stable up to 10 GPa (Schmidt & Poli, 1998). As was shown before, an enriched OIB source component is also suggested for the back-arc (SR) zone. However, the enrichment in LREE/HREE occurs mainly from EVF to CKD (Fig. 13). This is apparently due to a reduction in the degree of partial melting (see above). However, Sr isotope ratios in CKD rocks indicate that additional enrichment exists, which could result from the effect of dehydration of lawsonite deeper in the slab.

Slab melts in the source of the NCKD volcanoes

NCKD samples (Shiveluch, Zarechny, Kharchinsky) are considered separately as they display distinct trace element patterns. They have high $(Sr/Y)_{6\cdot0}$ ratios of ~35 and $(La/Yb)_{6\cdot0}$ of ~5 (Fig. 7a and d), which by far exceeds compositions on the across-arc trend. Such a pattern is typical for adakites, which are assumed to be derived from slab melting (Defant & Drummond, 1990). The unusually high values of $(SiO_2)_{6\cdot0}$, $(K_2O)_{6\cdot0}$ and $(Na_2O)_{6\cdot0}$ also are in favour of an alkali-rich adakitic component in the NCKD lavas. HFSE contents in the NCKD and the 'normal' CKD rocks are similar and indicate that the HFSE were not significantly contributed by the slab melt component. This implies that residual

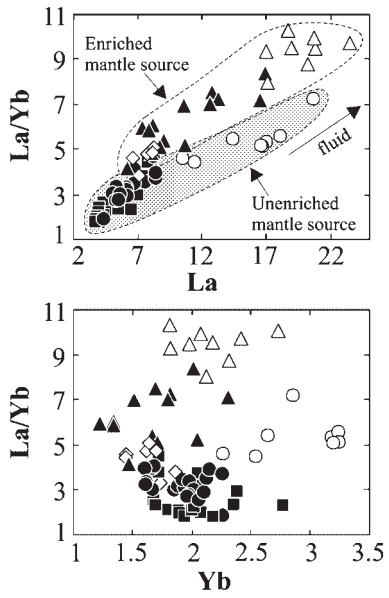

Fig. 13. La/Yb vs La and Yb showing that increasing La/Yb from the frontal zone to the back-arc is a result of increase in La at constant Yb concentrations. Symbols as in Fig. 2.

sphene or rutile with high $D_{\text{mineral/melt}}$ for the HFSE must have retained these elements in the slab. The origin of the adakite-type signatures was related to the special plate configuration below the NCKD volcanoes, by Volynets *et al.* (1997*b*) and Yogodzinski *et al.* (2000). Those workers proposed that the Pacific plate is torn and superimposed by hot asthenospheric mantle below the NCKD volcanoes, which are located directly along the extension of the subducted transform boundary between the Pacific and Komandorsky plates. In this scenario the Pacific plate is surrounded and heated by hot mantle from three sides, causing it to melt and to provide the adakite component to the mantle source of NCKD volcanoes.

High-K calc-alkaline basalts of the CKD

High-K calc-alkaline basalts occur at Tolbachik and Ploskie Sopky volcanoes in the Kluchevskaya Group together with 'normal' medium-K calc-alkaline volcanic rocks. Compared with the latter, they are enriched in all incompatible elements, except Sr (Fig. 3) and therefore also fall off the across-arc trend in most geochemical parameters. The trace element patterns of the high-K calc-alkaline rocks are parallel to those of the other CKD rocks, which suggests that they could be derived from a similar source.

In detail, however, the high-K calc-alkaline rocks are displaced from the CKD rocks to an enriched composition with higher Ta/Yb and Th/Yb ratios (Fig. 12). Also, the K/Rb ratios are significantly lower in the high-K calc-alkaline rocks. The lower Sr- and Pb-isotopic ratios in the high-K calc-alkaline basalts compared with the other CKD rocks also are in favour of a different source. An OIB component in the source such as for SR rocks is not likely, on the basis of the low HFSE contents. The observed difference in HFSE could be explained by a relatively less depleted source for CKD calc-alkaline rocks compared with the other suites. Larger amounts of slab fluid could be responsible for the stronger enrichment of other incompatible elements and $^{87}Sr/^{86}Sr$ isotopes.

The high-K calc-alkaline rocks of the CKD therefore had a more fluid-enriched mantle source compared with other rocks of the Kluchevskaya Group, but this enrichment is not associated with an OIB component.

A model for magma generation across the Kamchatka arc

An evaluation of the fluid composition using Pearce (1983) and Pearce & Parkinson (1993) is summarized in Fig. 14a. This approach is based on the assumption that the fluid does not carry any significant amount of HFSE and HREE. The fluid-absent source patterns can then be estimated by fitting a line through the HFSE and HREE concentrations in a normalized trace element variation diagram (dashed line in Fig. 15). For this approach, we use only compositions with >5% MgO to avoid the influence of (plagioclase) crystallization on Ba, Rb, Sr and K (Fig. 4). The difference between this pattern and the rock composition gives the subduction component (Pearce, 1983). Our results show that the subduction component patterns for our six rock suites from Kamchatka are surprisingly similar, except for somewhat lower Sr in high-K CKD rocks.

Figure 14b illustrates the percentage of the subduction component (or mantle wedge) contributed to the magma for each element for different rock suites from the transect. The highest contribution is observed for LILE, decreasing to LREE and further to MREE, which were mainly derived from the mantle source. The WPT and, for some elements, SR (IAB) rocks show higher contributions of elements from the (enriched?) mantle component compared with EVF and CKD lavas.

Having determined this fluid pattern, we now turn to the mantle composition as defined by fluid immobile elements in the trace element variation diagrams. We have shown above that different mantle sources are involved in magma generation in the Kamchatka arc. For EVF and CKD (except NCKD) rocks all the incompatible mantle-derived elements (HREE, Nb, Ta, Ti, Y) form a trend parallel to, but below the N-MORB pattern. Such low concentrations of trace elements could be the result of large degrees of melting relative to N-MORB as well as some degree of prior depletion of the MORB source

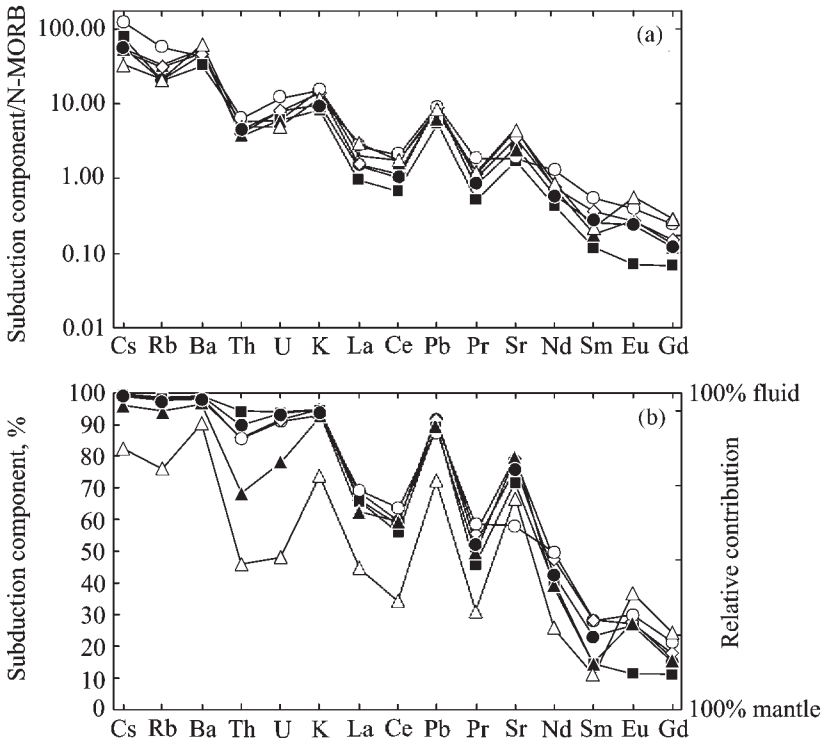

Fig. 14. (a) N-MORB-normalized trace element patterns of the subduction component estimated for the volcanic suites of the Kamchatka rocks, after Pearce (1983). N-MORB values are after Sun & McDonough (1989). It should be noted that the patterns for the six Kamchatka rock suites are surprisingly similar. Details of calculations are given in the text. (b) The percentage of the subduction component for each element in the rock. The highest contribution from the subduction component is found for LILE, and lesser contributions for LREE and MREE, which were mainly derived from the mantle. WPT and (for some elements) SR island-arc basalts rocks show a larger contribution for some elements from an enriched mantle source. Symbols as in Fig. 2.

(<5% melt lost, after Pearce & Parkinson, 1993). From these elements, which can be assumed to be little affected by subducted fluids, we start our model for magma generation across Kamchatka, as follows.

(1) We recalculated observed trace element patterns of the lavas to primitive, mantle-derived compositions. It is known that melts that are in equilibrium with mantle olivine have *mg*-number 0·68–0·75. In our transect such rocks occur in the CKD and in NCKD series. For others suites the highest *mg*-numbers range between 0·58 and 0·64 as a result of fractionation of olivine and pyroxene. Trace element compositions of the melts were re-calculated to primitive values at *mg*-number = 0·70, using microprobe mineral compositions from the same rocks (Dorendorf *et al.*, 1999, unpublished data).

(2) From the HFSE and HREE we approximate the melt trace element pattern for a mantle source without slab-fluid enrichment. Patterns obtained are very different for the different suites across Kamchatka (dashed lines in Fig. 15), suggesting variable mantle sources before slab-fluid enrichment.

(3) This source was then modelled by a combination of (a) a variably depleted N-MORB source, (b) an OIB component in the back-arc, and (c) a slab melt component for NCKD. Depletion factors relative to N-MORB source were derived from the relative HREE concentrations of N-MORB and our arc basalts, and are 1/1·9 for EVF, 1/1·7 for CKD medium-K, 1/0·3 for CKD high-K, 1/1·6 for NCKD, 1/1·8 for SR (IAB) and 1/1·4 for SR (WPT).

(4) An OIB composition after Sun & McDonough (1989) was used from which an OIB-source was calculated assuming that OIB is produced by 6% of batch melting of a garnet lherzolite. The sources for SR (IAB) and SR (WPT) were calculated as a mixture of 5% OIB-source and 95% N-MORB/1·8-source, and 35% OIB-source and 65% N-MORB/1·4-source. The enriched component for NCKD (slab melt) was calculated as 20% of batch melting of N-MORB with eclogite residue (Cpx/Gr = 50/50). The NCKD source before the addition of the subduction component was calculated as a mixture of 0·4% of such slab melt and an N-MORB/1·6-source.

(5) The concentrations used in the model for Ba, Nb and Pb in a H_2O-rich subduction component for our model were taken from Brenan *et al.* (1995); all other

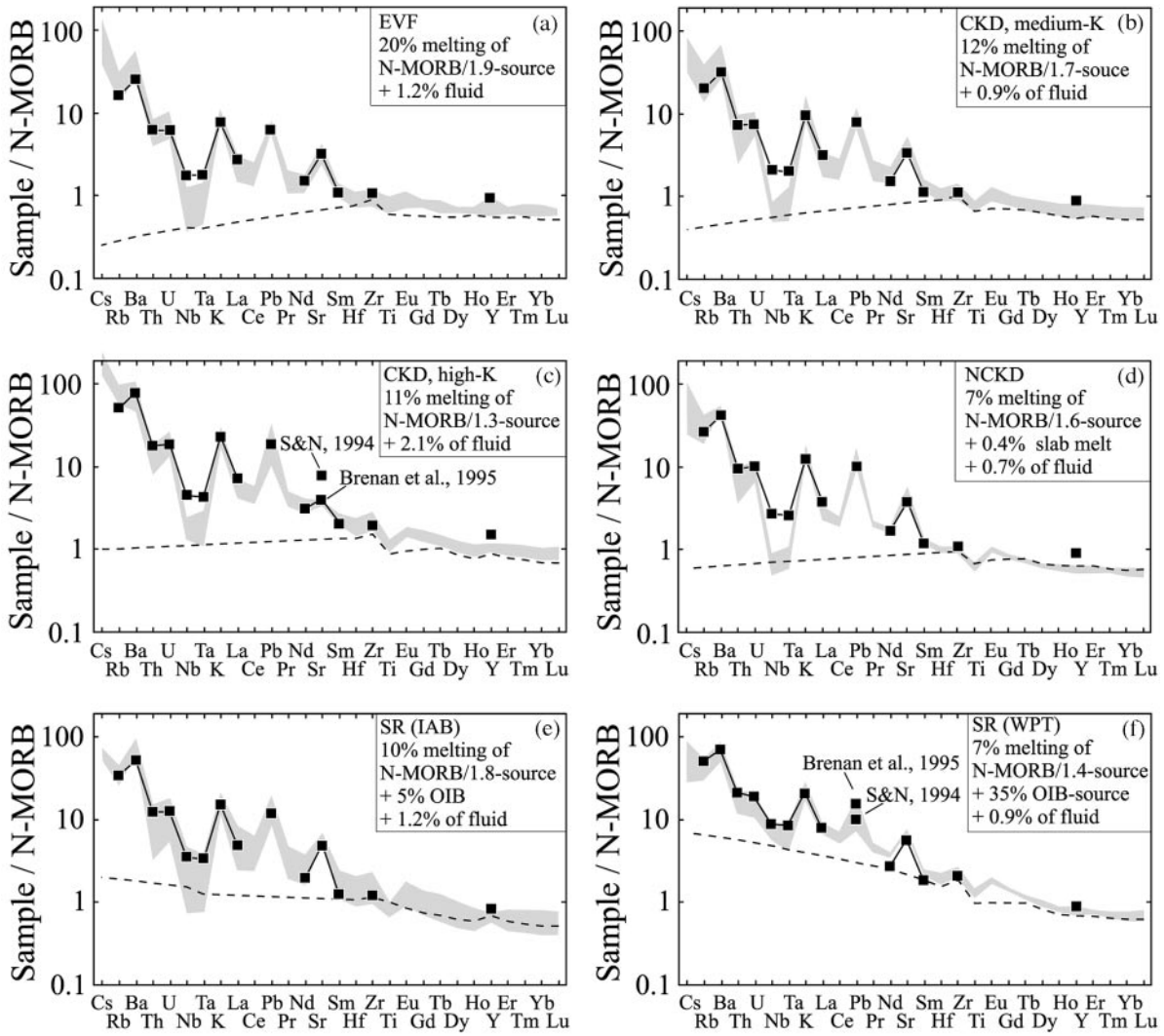

Fig. 15. Calculated magma compositions (■) based on a mixture of variably depleted mantle and variable amounts of a slab fluid composition from Stolper & Newman (1994) (S&N, 1994), except for Ba, Nb and Pb, which were also taken from Brenan *et al.* (1995). Dashed line shows the approximated patterns without the subduction enrichment. The melts derived from the enriched mantle sources were then calculated from a mixture of mantle wedge source (depleted by a given factor relative to N-MORB source) plus an OIB source component after Sun & McDonough (1989) for SR and a calculated slab melt for NCKD rocks. The proportions of mixtures in the source are shown in the inset. (For details see text.)

elements in the slab fluid are from Stolper & Newman (1994).

To model the actual rock trace element patterns we added this slab-fluid component in different proportions to the mantle source (spinel lherzolite) as calculated above and then calculated trace element patterns by batch melting this mantle to different degrees according to the $(CaO)_{6{\cdot}0}$–$(Na_2O)_{6{\cdot}0}$ systematics. The calculated patterns are shown in Fig. 15 for comparison with the recalculated primitive magma compositions (shaded areas). The amount of the subduction component required changes only slightly (from 0·7% to 1·2%); only CKD high-K rocks require twice this amount (2·1%).

Calculated concentrations for Ta, Nb and La are too high compared with EVF samples. The mismatch is smaller in rocks of the CKD. For the SR suites our calculated and observed values are in good agreement. Deviations could reflect minor differences in fluid composition from the front-arc zone to the back-arc. Whereas the fluid below EVF is poor in Ta, Nb and La, the fluid below the CKD is more enriched in La and the deep fluid below the SR is somewhat more enriched in all these elements. Because the calculated data for Y are too high we argue that the subduction component below Kamchatka has only insignificant amounts of this element, less than predicted by Stolper & Newman (1994).

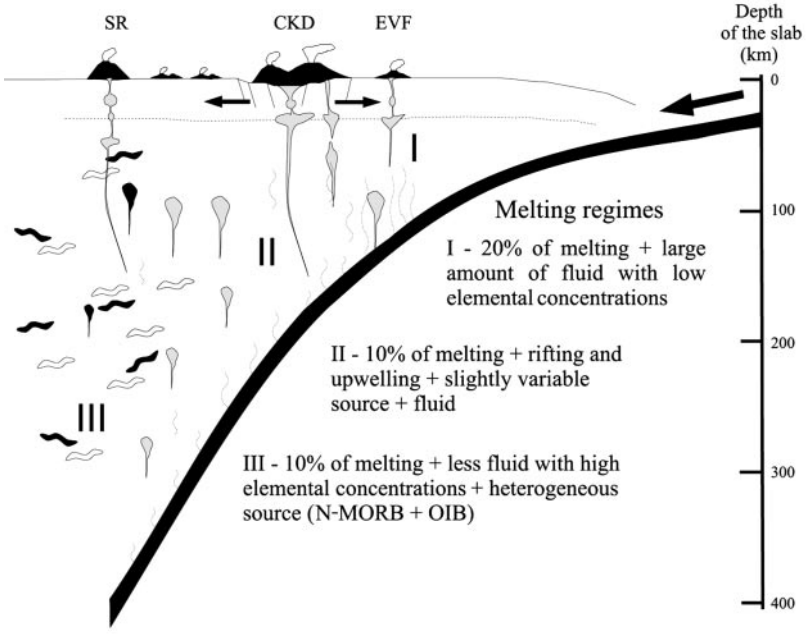

Fig. 16. Schematic model showing the relationship between the factors that influence the observed geochemical zonation in the Kamchatka transect. Melting in EVF and SR is dominated by the fluid flux, derived from the subducted slab and the Hawaii–Emperor Seamounts chain. The high magma production rate in the CKD zone is strongly affected by both slab dehydration and upwelling as a result of intra-arc rifting.

The CKD high-K rocks have a lower Sr contribution from the H_2O-rich fluid than other rocks (Figs 14 and 15c). A Sr fluid concentration as proposed by Brenan *et al.* (1995) would better fit our patterns. Pb concentrations calculated after Stolper & Newman (1994) are more acceptable for the WPT lavas. Dorendorf *et al.* (2000*a*) modelled a fluid component in the source of some high-$\delta^{18}O$ lavas from Kluchevskoy of up to almost 20% from $\delta^{18}O$–$^{87}Sr/^{86}Sr$ relations. This apparent contradiction to our estimate of fluid contributions to the source is resolved by the following observations: (1) the conclusion by Dorendorf *et al.* applies only to lavas with anomalously high $\delta^{18}O$ values, which were not specifically modelled here; (2) the fluid added in their model is not itself involved in the melting process (see the U-series argument above); (3) fluids of different solute content and O-isotope composition may need to be considered. The unusual high-$\delta^{18}O$ magmas documented by Dorendorf *et al.* (2000*a*) may thus represent large and multiple fluid inputs into the source, which on average had a low solute concentration.

The subduction component involved in magma generation for all Kamchatka samples, however, could be explained by either (1) the same amount of the same fluid or (2) different amounts of such fluid with variable trace element content but similar trace element patterns. Deep fluids below SR are likely to be more enriched in incompatible elements, as a result of the higher *P–T* conditions and breakdown of high-temperature minerals. Recently, Bureau & Keppler (1999) showed that fluids derived from the amphibole dehydration would be water rich, low in silica, and high in LILE and probably chloride. Such fluid could be very mobile, producing a large amount of melt, as in the EVF and CKD. Nevertheless, deep fluids (>100 km depth) derived from the breakdown of lawsonite would be poorer in water but richer in silica, and probably could transport significant amounts of HFSE. Such fluids are more viscous and less mobile. However, as La/Nb correlates positively with $^{143}Nd/^{144}Nd$ ratios for SR rocks (plot not shown) this suggests that the same component influences both ratios. This component thus could not simply be an HFSE-rich fluid, because the rocks of the SR in the Sr–Nd isotope diagram form a separate field of low $^{143}Nd/^{144}Nd$ at slightly higher $^{87}Sr/^{88}Sr$ (Fig. 9). Fluids from altered subducted oceanic crust are expected to have $^{143}Nd/^{144}Nd$ values close to those of N-MORB and thus should cause a shift only to higher $^{87}Sr/^{88}Sr$, as is observed for CKD rocks (Fig. 9).

As a result, we observe a fluid signature that is rather similar from front to back-arc, however, with increasing contributions for Nb and Ta (see above). In addition, we found that boron and chalcophile elements are also strongly correlated with slab depth and change significantly across the arc (Leeman *et al.*, 2001). This is consistent with our previous assumption that Kamchatka

magmas along our transect are mostly influenced by fluids from subducted oceanic basalts (crust and seamounts) rather than sediments.

The degree of melting in the model changes from 9–12% (for SR and CKD) to 20% (for EVF), which corresponds to worldwide published data for volcanic arcs. It is most likely that the higher degree of melting in the EVF is caused by a larger amount of water-rich fluid, derived from the first stage of slab dehydration. The subduction of the Hawaii–Emperor Seamounts could play an important role in fluid release in this volcanic zone. Comparison of our data for the EVF with published data on southern Kamchatka volcanoes (Castellana, 1998; Dorendorf *et al.*, 2001) shows that lavas in our transect are lower in most incompatible elements, which could be the result of a higher degree of melting in this zone. Southern EVF rocks are also higher in $^{206}Pb/^{204}Pb$. Leg 145 sediments [for compilation, see Kersting & Arculus (1995)] drilled off the Kamchatka trench are higher in ^{208}Pb, ^{206}Pb and ^{207}Pb, whereas the data of Castellana (1998) for the southern Avachinsky transect are shifted only to higher $^{206}Pb/^{204}Pb$. Also, in Sr–Nd isotope space, the compositions south of our transect tend to be more MORB-like (Castellana, 1998). This may be due to a distinct mantle wedge composition and a smaller fluid contribution in the south. As was shown before, rocks from Bakening volcano are also less radiogenic in Sr than northern EVF lavas. These observations underline the distinct character of our transect rocks and emphasize the probable role of the subduction of the seamount chain there.

The CKD also has the highest magma production across the arc, in fact for any arc worldwide. The reason for this could be related to intra-arc rifting and mantle upwelling in this area. Even if the degree of melting is not very high (~12% of partial melting), a large volume of mantle could be involved in this melting, as a result of massive decompression below the rift. Therefore the high magma production rate in CKD is caused by two factors: (1) intra-arc rifting, following upwelling and enhanced decompression melting; (2) enhanced fluid flux from the Emperor Seamounts chain.

Obviously, many of the choices made in this multicomponent model are somewhat arbitrary. However, limited variations in the compositions and parameters do not affect the basic conclusions, which are as follows:

(1) the mantle wedge below Kamchatka is depleted by a factor of 1·3–1·9 relative to the source of N-MORB;

(2) an enriched, OIB-source component (5–35%) is required in the mantle source of the back-arc;

(3) a slab-derived melt in the source of NCKD volcanoes is consistent with their geochemical characteristics;

(4) degrees of melting range from 20% at the front to ≤10% in the back-arc;

(5) the character of the slab signature shows only minor changes across the arc for the elements studied here (see, however, Leeman *et al.*, 2001);

(6) the amount of fluid ranges from 1·2% at the front to >2% below the CKD;

(7) slight difference exist in HFSE content of the fluid (higher in the back-arc).

CONCLUSIONS

(1) Major and trace element as well as Sr–Nd–Pb isotope compositions of mafic rocks from Kamchatka show systematic variations from the volcanic arc front at Komarov volcano to the back-arc at Ichinsky volcano, and indicate the involvement of distinct sources.

(2) Three parameters have mainly affected the observed geochemical zonation across the arc: (a) variably depleted and enriched mantle sources; (b) the fluid flux from the slab to the mantle wedge; (c) variable degrees of melting.

(3) Variably depleted mantle sources exist below Kamchatka, from slightly depleted (EVF, CKD) to significantly enriched (SR) compared with an N-MORB source. The depletion is possibly related to earlier MORB- or intra-arc rifting and melting events, which produced, for example, extensive plateau basalts and andesites in the Lower Pleistocene.

(4) The within-plate type basalts in the SR contain a significant contribution of an HFSE-enriched OIB source component (~35%) in their source. The other rocks of the SR have up to 5% OIB source component in their source.

(5) The contribution from the slab is nearly identical in fluid mobile trace elements such as Ba, Pb and LREE, except for variations in chalcophile elements (Leeman *et al.*, 2001) across the arc. In particular, high-K CKD rocks have higher fluid flux, and higher U/Th, $^{87}Sr/^{86}Sr$ and Ba/Zr ratios.

(6) An influence from slab-derived melts is found for the NCKD volcanoes (Shiveluch, Kharchinsky and Zarechny), where it is caused by superimposing hot mantle wedge and subducted slab along the northern edge of the Pacific plate.

(7) The slab fluids were mostly derived from dehydration of subducted basalts; a sediment component is not apparent.

(8) The relatively large fluid flux from the subducted seamount basalts and the intra-arc rifting caused the high magma production rate observed in the CKD rocks of the Kluchevskaya Group.

ACKNOWLEDGEMENTS

Jon Davidson and Phil Kyle are thanked for their detailed and constructive reviews. Oleg Volynets (deceased) shared

freely his ideas and data about Kamchatka magmatism and gave invaluable hints for sampling some of the most remote volcanoes. We are very grateful to K. Eusterhues, A. Koloskov and G. Flerov for help and collaboration during the fieldwork. Support was provided by DFG-project Wo362/15-1+2 and the Volkswagen-Foundation to G.W., by INTAS-Co-operation Project Grant 94-3129 to Clive Oppenheimer (Bristol) and T.C., and Grant 98-05-04103 from the DFG-RFBR Co-operation Programme.

REFERENCES

Arculus, R. J. (1994). Aspects of magma genesis in arcs. In: Arculus, R. J., Banno, S., Charvet, J. & Kushiro, I. (eds) *Tectonics, Metamorphism and Magmatism in Island Arcs. Lithos* **33**(1–3), 189–208.

Avdeiko, G. P., Volynets, O. N., Antonov, A. Y. & Tsvetkov, A. A. (1991). Kurile island-arc volcanism; structural and petrological aspects. In: Zonenshain, L. P. (ed.) *The Achievements of Plate Tectonics in the USSR. Tectonophysics* **199**, 271–287.

Ayers, J. (1998). Trace element modeling of aqueous fluid–peridotite interaction in the mantle wedge of subduction zones. *Contributions to Mineralogy and Petrology* **132**, 390–404.

Ayers, J. C., Dittmer, S. K. & Layne, G. D. (1997). Partitioning of elements between peridotite and H_2O at 2·0–3·0 GPa and 900–1100 degrees C, and application to models of subduction zone processes. *Earth and Planetary Science Letters* **150**, 381–398.

Balesta, S. T. (1991). Earth crust structure and magma chambers of the areas of present Kamchatka volcanism. In: Fedotov, S. A. & Masurenkov, Y. P. (eds) *Active Volcanoes of Kamchatka*. Moscow: Nauka, pp. 36–45.

Baranov, B. V., Seliverstov, N. I., Muravev, A. V. & Muzurov, E. L. (1991). The Komandorsky Basin as a product of spreading behind a transform plate boundary. In: Zonenshain, L. P. (ed.) *The Achievements of Plate Tectonics in the USSR. Tectonophysics* **199**, 237–269.

Brenan, J. M., Shaw, H. F., Ryerson, F. J. & Phinney, D. L. (1995). Mineral–aqueous fluid partitioning of trace elements at 900 degrees C and 2·0 GPa; constraints on the trace element chemistry of mantle and deep crustal fluids. *Geochimica et Cosmochimica Acta* **59**, 3331–3350.

Bureau, H. & Keppler, H. (1999). Complete miscibility between silicate melts and hydrous fluids in the upper mantle; experimental evidence and geochemical implications. *Earth and Planetary Science Letters* **165**, 187–196.

Castellana, B. (1998). Geology, chemostratigraphy, and petrogenesis of the Avachinskiy Volcano, Kamchatka, Russia. Ph.D. thesis, University of California, Los Angeles, 365 pp.

Defant, M. J. & Drummond, M. S. (1990). Derivation of some modern arc magmas by melting of young subducted lithosphere. *Nature* **347**, 662–665.

Dorendorf, F. (1998). Genesis of Quaternary volcanic rocks from Kamchatka/Russia. Ph.D. thesis, Geochemisches Institut, Göttingen University, 132 pp.

Dorendorf, F., Wiechert, U. & Wörner, G. (2000a). Hydrated sub-arc mantle: a source for the Kluchevskoy volcano, Kamchatka/Russia. *Earth and Planetary Science Letters* **175**, 69–86.

Dorendorf, F, Churikova, T., Koloskov, A & Wörner, G. (2000b). Late Pleistocene to Holocene activity at Bakening volcano and surrounding monogenetic centers (Kamchatka): volcanic geology and geochemical evolution. *Journal of Volcanology and Geothermal Research* **104**, 131–151.

Fedotov, S. A. (1991). On the mechanism of volcanic activity in Kamchatka, Kuril–Kamchatka arc and in similar structures. In: Fedotov, S. A. & Masurenkov, Y. P. (eds) *Active Volcanoes of Kamchatka*. Moscow: Nauka, pp. 30–35.

Geist, E. L. & Scholl, D. W. (1994). Large-scale deformation related to the collision of the Aleutian Arc with Kamchatka. *Tectonics* **13**, 538–560.

Gorbatov, A. V. (1997). Sismicidad y estructura de la zona de subduction de Kamchatka. Ph.D. thesis, Instituto de Geofisica, UNAM, Mexico City, 144 pp.

Gorelchik, V. I., Shirokov, V. A., Firstov, P. P. & Chubarova, O. S. (1997). Shiveluch Volcano; seismicity, deep structure and forecasting eruptions (Kamchatka). *Journal of Volcanology and Geothermal Research* **78**, 121–137.

Hochstaedter, A. G., Kepezhinskas, P., Defant, M., Drummond, M. & Koloskov, A. (1996). Insights into the volcanic arc mantle wedge from magnesian lavas from the Kamchatka Arc. *Journal of Geophysical Research, B, Solid Earth and Planets* **101**, 697–712.

Hofmann, A. W. (1988). Chemical differentiation of the Earth; the relationship between mantle, continental crust, and oceanic crust. In: Welin, E. (ed.) *Isotope Geochemistry; the Crafoord Symposium. Earth and Planetary Science Letters* **90**, 297–314.

Kepezhinskas, P., McDermott, F., Defant, M. J., Hochstaedter, A., Drummond, M. S., Hawkesworth, C. J., Koloskov, A., Maury, R. C. & Bellon, H. (1997). Trace element and Sr–Nd–Pb isotopic constraints on a three-component model of Kamchatka Arc petrogenesis. *Geochimica et Cosmochimica Acta* **61**, 577–600.

Kersting, A. B. & Arculus, R. J. (1995). Pb isotope composition of Klyuchevskoy Volcano, Kamchatka and North Pacific sediments; implications for magma genesis and crustal recycling in the Kamchatkan arc. *Earth and Planetary Science Letters* **136**, 133–148.

Leeman, W., Wörner, G., Churikova, T., Tonarini, S. & Heuser, A. (2001). Boron and fluid-mobile element (FME) fluxes across Kamchatka. *EUG 11*. Strasbourg 2001. *Journal of Conference Abstracts* **6**, 391.

Le Maitre, R. W., Bateman, P., Dudek, A., Keller, J., Lameyre, Le Bas, M. J., Sabine, P. A., Schmid, R., Sorensen, H., Streckeisen, A., Woolley, A. R. & Zanettin, B. (1989). *A Classification of Igneous Rocks and Glossary of Terms*. Oxford: Blackwell.

Luchitsky, I. V. (1974). *Kamchatka, Kurile and Commander Islands*. Moscow: Nauka (in Russian).

McCulloch, M. T. & Gamble, A. J. (1991). Geochemical and geodynamical constraints on subduction zone magmatism. *Earth and Planetary Science Letters* **102**, 358–374.

Melekestsev, I. V., Khrenov, A. P. & Kozhemyaka, N. N. (1991). Tectonic position and general description of volcanoes of Northern group and Sredinny Range. In: Fedotov, S. A. & Masurenkov, Y. P. (eds) *Active Volcanoes of Kamchatka*. Moscow: Nauka, pp. 74–81.

Melzer, S. & Wunder, B. (2000). Island-arc basalts alkali ratios: constraints from phengite–fluid partitioning experiments. *Geology* **28**(7), 583–586.

Miller, D. M., Goldstein, S. L. & Langmuir, C. H. (1994). Cerium/lead and lead isotope ratios in arc magmas and the enrichment of lead in the continents. *Nature* **368**, 514–520.

Minster, J. B. & Jordan, T. H. (1978). Present-day plate motions. *Journal of Geophysical Research* **83**, 5331–5354.

Pearce, J. A. (1983). Role of the sub-continental lithosphere in magma genesis at active continental margins. In: Hawkesworth, C. J. & Norry, M. J. (eds) *Continental Basalts and Mantle Xenoliths; Papers Prepared for a UK Volcanic Studies Group Meeting at the University of Leicester*. Nantwich: Shiva, pp. 230–249.

Pearce, J. A. & Parkinson, I. J. (1993). Trace element models for mantle melting; application to volcanic arc petrogenesis. In: Prichard, H.

M., Alabaster, T., Harris, N. B. W. & Neary, C. R. (eds) *Magmatic Processes and Plate Tectonics. Geological Society, London, Special Publications* **76**, 373–403.

Plank, T. & Langmuir, C. H. (1988). An evaluation of the global variations in the major element chemistry of arc basalts. *Earth and Planetary Science Letters* **90**, 349–370.

Plank, T. & Langmuir, C. H. (1993). Tracing trace elements from sediment input to volcanic output at subduction zones. *Nature* **362**, 739–743.

Schmidt, M. W. & Poli, S. (1998). Experimentally based water budgets for dehydrating slabs and consequences for arc magma generation. *Earth and Planetary Science Letters* **163**, 361–379.

Shibata, T. & Nakamura, E. (1997). Across-arc variations of isotope and trace element compositions from Quaternary basaltic volcanic rocks in northeastern Japan; implications for interaction between subducted oceanic slab and mantle wedge. *Journal of Geophysical Research, B, Solid Earth and Planets* **102**, 8051–8064.

Stalder, R., Foley, S. F., Brey, G. P. & Horn, I. (1998). Mineral–aqueous fluid partitioning of trace elements at 900°C–1200°C and 3·0 GPa to 5·7 GPa: new experimental data for garnet clinopyroxene and rutile and implications for mantle metasomatism. *Geochimica et Cosmochimica Acta* **62**, 1781–1801.

Stolper, E. & Newman, S. (1994). The role of water in the petrogenesis of Mariana Trough magmas. *Earth and Planetary Science Letters* **121**, 293–325.

Sun, S. S. & McDonough, W. F. (1989). Chemical and isotopic systematics of oceanic basalts; implications for mantle composition and processes. In: Saunders, A. D. & Norry, M. J. (eds) *Magmatism in the Ocean Basins. Geological Society, London, Special Publications* **42**, 313–345.

Tatsumi, Y. & Eggins, S. (1995). *Subduction Zone Magmatism. Frontiers in Earth Sciences*. Oxford: Blackwell Science.

Tatsumi, Y., Kogiso, T. & Nohda, S. (1995). Formation of a third volcanic chain in Kamchatka; generation of unusual subduction-related magmas. *Contributions to Mineralogy and Petrology* **120**, 117–128.

Todt, W., Cliff, R. A., Hanser, A. & Hofmann, A. W. (1984). ^{202}Pb–^{205}Pb spike for Pb isotope analysis. *Terra Cognita* **4**, 209.

Tribuzio, R., Messiga, B., Vannucci, R. & Bottazzi, P. (1996). Rare earth element redistribution during high-pressure–low-temperature metamorphism in ophiolitic Fe-gabbros (Liguria, northwestern Italy); implications for light REE mobility in subduction zones. *Geology* **24**, 711–714.

Tsvetkov, A. A., Gladkov, N. G. & Volynets, O. N. (1989). Problem of sediment subduction and ^{10}Be isotope in lavas of Kuril Islands and Kamchatka Peninsula. *Doklady Akademii Nauk SSSR* **306**, 1220–1225.

Turner, S., McDermott, F., Hawkesworth, C. & Kepezhinskas, P. (1998). A U-series study of lavas from Kamchatka and the Aleutians: constraints on source composition and melting processes. *Contributions to Mineralogy and Petrology* **133**, 217–234.

Volynets, O. N. (1994). Geochemical types, petrology, and genesis of late Cenozoic volcanic rocks from the Kurile–Kamchatka island-arc system. *International Geology Review* **36**, 373–405.

Volynets, O. N., Karpenko, S. F., Kay, R. W. & Gorring, M. (1997*a*). Isotopic composition of Late Neogene K–Na alkaline basalts of Eastern Kamchatka: indicators of the heterogeneity of the mantle magma sources. *Geochemistry International* **35**, 884–896.

Volynets, O., Wörner, G., Babansky, A., Dorendorf, F., Churikova, T., Yogodzinski, G., Goltsman, Y. & Agapova, A. (1997*b*). Variations in geochemistry and Sr–Nd isotopes in lavas from the Northern Volcanic Group, Kamchatka; evidence for distinct sources at a subducting transform system. *EOS Transactions, American Geophysical Union* **78**, F804.

Yogodzinski, G. M., Lees, J. M., Churikova, T. G., Dorendorf, F., Wörner, G. & Volynets, O. N. (2000). Slab edge geochemical effects on arc magmatism and the torn Pacific Plate beneath Kamchatka and the Western Aleutians. *Nature* **409**, 500–504.

Zindler, A. & Hart, S. (1986). Chemical geodynamics. *Annual Review of Earth and Planetary Sciences* **14**, 493–571.